Discrete gradient flows for general curvature energies

Willy Dörfler, Robert Nürnberg

KARLSRUHE INSTITUTE OF TECHNOLOGY

CRC 1173

Participating universities

Universität Stuttgart

EBERHARD KARLS
UNIVERSITÄT
TÜBINGEN

Funded by

DFG

Discrete gradient flows
for general curvature energies

Willy Dörfler[*]   Robert Nürnberg[†]

Abstract

We consider the numerical approximation of the L^2–gradient flow of general curvature energies $\int G(|\vec{\varkappa}|)$ for a curve in $\mathbb{R}^d$, $d \geq 2$. Here the curve can be either closed, or it can be open and clamped at the end points. These general curvature energies, and the considered boundary conditions, appear in the modelling of the power loss within an optical fibre. We present two alternative finite element approximations, both of which admit a discrete gradient flow structure. Apart from being stable, in addition, one of the methods satisfies an equidistribution property. Numerical results demonstrate the robustness and the accuracy of the proposed methods.

Key words. curvature energy, gradient flow, clamped boundary conditions, finite element approximation, equidistribution, optical fibre.

AMS subject classifications. 65M60, 65M12, 35K55, 53C44, 74E10

1 Introduction

The classical elastic energy of a curve is defined by the integral of the squared norm of the curvature $\vec{\varkappa}$. This energy, as a model for the elastic energy of a rod, has been first considered and analysed by Bernoulli (1738) and Euler (1743), see Euler (1952). Further, and more recent, applications for this energy are the modelling of DNA rings and other curved nanostructures, see Goyal *et al.* (2005); Tu and Ou-Yang (2008); and edge completion in computer vision, see Mio *et al.* (2004).

In this paper we study the L^2–gradient flow of curvature energies that depend in a more general form on $\vec{\varkappa}$. Such energies appear, for example, when one studies the power loss within an optical fibre that acts as a wire bond, i.e. as an interchip connection, where

---

[*]Institut für Angewandte und Numerische Mathematik, Karlsruher Institut für Technologie (KIT), 76049 Karlsruhe, Germany

[†]Department of Mathematics, Imperial College London, London, SW7 2AZ, UK

data is transmitted by light between different components of the chip, see Lindenmann *et al.* (2012). Since these connections are long and thin, a common modelling approach is to formulate the losses in terms of geometrical quantities of a connecting curve. More specifically, the energy we are going to consider is defined by

$$\int [G(|\vec{\varkappa}|) + \lambda]\,, \tag{1.1}$$

where $G(|\kappa|)$ is the optical loss per length due to the bending of the wire bond, while $\lambda > 0$ models the optical loss per length of the connection. If P_{in} and P_{out} denote the incoming and outgoing power, respectively, then the loss in this model is given by

$$\frac{P_{\text{in}} - P_{\text{out}}}{P_{\text{in}}} = 1 - \exp\left(-2\int [G(|\vec{\varkappa}|) + \lambda]\right), \tag{1.2}$$

and so minimising the loss is equivalent to minimising the energy (1.1). Examples for functions G of interest are

$$G(z) = \tfrac{1}{p}\, z^p\,, \qquad p \in (1, \infty)\,, \tag{1.3a}$$

$$G(z) = e^{-\alpha/z}\,, \qquad \alpha \in (0, \infty)\,, \tag{1.3b}$$

$$G(z) = \sqrt{z}\, e^{-\alpha/z}\,, \quad \alpha \in (0, \infty)\,. \tag{1.3c}$$

The case (1.3a) with $p = 2$ leads to the classical elastic energy, while a physical interpretation for (1.3a) with $p \in (1, \infty)$ in connection with losses in optical fibres is given in Baets and Lagasse (1983, (16)) and Koos *et al.* (2007, p. 819) ($d = 2$). The choices (1.3b)–(1.3c) are in the same connection advocated in Marcuse (1993, (14)) for $d = 2$ and in Marcuse (1993, (34)) for $d = 3$. While these (approximative) formulas were originally derived for constantly curved slabs or fibres, they are also used for trajectories with slowly varying curvature. In applications one would provide two contact points for the wire, and a prescribed direction for the wire at each endpoint. These boundary conditions are called "clamped boundary conditions". A more realistic model of wire bonds would include also the "transition loss" caused by varying curvature in (1.2). However, a corresponding term in the energy (1.1), that models the transition loss, is not known to this date. In Negredo *et al.* (2018) such a wire bond connection in the plane was optimised with respect to its loss by using (1.1), but with transition losses calculated from the interpolation of precomputed values. In this paper we will neglect transition losses and concentrate on (1.1) instead.

Of course, for the choice (1.3a) with $p = 2$ the energy (1.1) reduces to the classical elastic energy, and its L^2–gradient flow is called elastic flow. The classical case is by now well studied both analytically and numerically. For theoretical results we refer to Polden (1996); Dziuk *et al.* (2002); Deckelnick and Grunau (2007, 2009); Schätzle (2010); Dall'Acqua *et al.* (2017), while numerical approximations have been considered in Dziuk *et al.* (2002); Deckelnick and Dziuk (2009); Barrett *et al.* (2010, 2012). A scheme for the elastic flow of inextensible curves has been proposed and analysed in Bartels (2013); Bartels *et al.* (2018). Here we stress that in Deckelnick and Dziuk (2009) a first stability

result for a discretisation of elastic flow was presented, together with an error analysis. In Barrett *et al.* (2012) an alternative discretisation was presented, that can also be shown to be stable, and that, in addition, satisfies an equidistribution property.

It the the aim of this paper to extend the stability results in Deckelnick and Dziuk (2009); Barrett *et al.* (2012) to the more general energy (1.1). In applications one is often interested in the minimising shape of the curve. Here we view the L^2–gradient flow as an opportune method to produce possible candidates. We stress that, to the best of our knowledge, so far there exist no results on the analysis or numerical analysis of gradient flows for the more general energy (1.1). Moreover, we will present exact radial solutions for the L^2–gradient flow of (1.1) for the choices in (1.3). Once again, we believe that these are the first such results in the literature. Finally, we remark that our theoretical and numerical results reveal the qualitatively very different behaviour of the evolution for the gradient flow for general G, compared to the classical case, when $G(z) = \frac{1}{2} z^2$. For example, while stationary solutions exist for (1.3a) for any $p \in (1, \infty)$ and $\lambda > 0$, there are no stationary solutions in the cases (1.3b) and (1.3c) if λ is sufficiently large.

The remainder of this paper is organised as follows. In the next section we introduce the precise mathematical formulations of the gradient flows we would like to study. In Section 3 we state two alternative weak formulations, and in Section 4 we introduce continuous-in-time semidiscrete finite element approximations based on these formulations. We show that our approximations satisfy a stability bound and prove an equidistribution property for one of the schemes. In Section 5 we introduce the corresponding fully discrete versions of the semidiscrete approximations derived in the previous section. At every time level, a nonlinear system has to be solved for the approximations, and we give details on a possible solution procedure. In Section 6 we report on numerous numerical experiments, which demonstrate the effectiveness of our fully discrete approximations. Moreover, convergence experiments, based on exact solutions that we derive in the appendix, show a quadratic convergence rate for our finite element approximations.

2   Mathematical formulation

Let either $I = \mathbb{R}/\mathbb{Z}$, the periodic interval $[0, 1]$, or $I = (0, 1)$. Note that in the former case we have $\partial I = \emptyset$, while in the latter case it holds that $\partial I = \{0, 1\}$. Let $\vec{x} : \overline{I} \to \mathbb{R}^d$ be a parametrisation of the curve $\Gamma \subset \mathbb{R}^d$, $d \geq 2$. Note that Γ is closed if $I = \mathbb{R}/\mathbb{Z}$ and open if $I = (0, 1)$. We also define the function spaces $\underline{V} = [H^1(I)]^d$ and $\underline{W} = [H_0^1(I)]^d$, and note that $\underline{W} = \underline{V}$ in the case $I = \mathbb{R}/\mathbb{Z}$.

On assuming that

$$|\vec{x}_\rho(\rho)| \geq c_0 > 0 \qquad \forall \, \rho \in I \,, \tag{2.1}$$

we introduce the arclength parameter s of the curve, i.e. $\partial_s = |\vec{x}_\rho|^{-1} \partial_\rho$, and define the

3

unit tangential vector field

$$\vec{\tau}(\rho) = \vec{x}_s(\rho) = \frac{\vec{x}_\rho(\rho)}{|\vec{x}_\rho(\rho)|}\,. \tag{2.2}$$

When we consider the evolution of open curves, we impose the clamped boundary conditions

$$\vec{x}(q) = \vec{\alpha}_q \quad \text{and} \quad (-1)^{q+1}\,\vec{\tau}(q) = \vec{\zeta}_q \quad \forall\, q \in \partial I\,, \tag{2.3}$$

for given $\vec{\alpha}_0, \vec{\alpha}_1 \in \mathbb{R}^d$ and $\vec{\zeta}_0, \vec{\zeta}_1 \in \mathbb{S}^{d-1} = \{\vec{p} \in \mathbb{R}^d : |\vec{p}| = 1\}$. The curvature vector $\vec{\varkappa}$ of Γ is given by

$$\vec{\varkappa} = \vec{\tau}_s = \vec{x}_{ss}\,, \quad \text{implying} \quad \vec{\varkappa} \cdot \vec{\tau} = 0\,. \tag{2.4}$$

Energy minimisation.   We are interested in minimisers of the energy

$$E_\lambda(\vec{x}) = \int_I \left[G(|\vec{\varkappa}|) + \lambda \right] |\vec{x}_\rho| \,\mathrm{d}\rho\,, \tag{2.5}$$

where $\lambda \in \mathbb{R}$ is a constant, subject to the boundary conditions (2.3), and with given energy density $G : \mathbb{R}_{\geq 0} \to \mathbb{R}_{>0}$. Variations Variations of (2.5) in $\vec{\varkappa}$ in the direction of a vector field $\vec{\eta}$, yield the term $\int_I G'(|\vec{\varkappa}|)\,|\vec{\varkappa}|^{-1}\,\vec{\varkappa} \cdot \vec{\eta}\,|\vec{x}_\rho|\,\mathrm{d}\rho$, and so unless there are further conditions on G, this term does not make sense for $\vec{\varkappa} \to \vec{0}$. A sufficient condition for this term to be well-defined is

$$G'(z) \to 0 \text{ as } z \to 0\,, \tag{2.6}$$

and we make that assumption from now on. Note that it is satisfied for the examples (1.3a)–(1.3c). Throughout this paper, we set

$$G'(|\vec{z}|)\,|\vec{z}|^{-1}\,\vec{z} = \vec{0} \quad \text{if} \quad \vec{z} = \vec{0}\,, \tag{2.7}$$

which is justified by (2.6).

Gradient flow.   In order to approach stationary points of (2.5) we will use a timedependent gradient flow. We begin by deriving the strong formulation of the L^2–gradient flow of (2.5). To this end, let $(\Gamma(t))_{t \in [0,T]}$ be a family of curves in $\mathbb{R}^d$, parameterised by $\vec{x} : \overline{I} \times [0,T] \to \mathbb{R}^d$, $(\rho, t) \mapsto \vec{x}(\rho, t)$. Straightforward calculations give, on recalling (2.4), that

$$(|\vec{x}_\rho|)_t = \vec{x}_s \cdot (\vec{x}_t)_\rho = \vec{\tau} \cdot (\vec{x}_t)_\rho\,, \tag{2.8a}$$

$$\vec{\tau}_t = |\vec{x}_\rho|^{-1}\,\underline{\underline{P}}\,\vec{x}_{\rho,t} = \vec{\nabla}_s\,\vec{x}_t\,, \tag{2.8b}$$

where the normal projection $\underline{\underline{P}}$ is defined by

$$\underline{\underline{P}} = \underline{\underline{\mathrm{Id}}} - \vec{\tau} \otimes \vec{\tau} \quad \text{and} \quad \vec{\nabla}_s = \underline{\underline{P}}\,\partial_s\,. \tag{2.9}$$

A weak formulation of (2.4), on noting (2.3), is given by

$$\int_I \vec{\varkappa} \cdot \vec{\eta}\,|\vec{x}|_\rho \,\mathrm{d}\rho + \int_I \vec{\tau} \cdot \vec{\eta}_\rho \,\mathrm{d}\rho = \sum_{q \in \partial I} \vec{\zeta}_q \cdot \vec{\eta}(q) \qquad \forall\, \vec{\eta} \in \underline{V}\,. \tag{2.10}$$

4

Note that $\vec{\eta}(q)$ is well-defined for $\vec{\eta} \in [H^1(I)]^d$. Differentiating (2.10) with respect to time yields

$$\int_I \vec{\varkappa}_t \cdot \vec{\eta} \, |\vec{x}|_\rho \, \mathrm{d}\rho + \int_I \vec{\varkappa} \cdot \vec{\eta} \, (|\vec{x}|_\rho)_t \, \mathrm{d}\rho + \int_I \vec{\tau}_t \cdot \vec{\eta}_\rho \, \mathrm{d}\rho = 0 \qquad \forall \, \vec{\eta} \in \underline{V} \,. \tag{2.11}$$

It follows from (2.11) and (2.8), and on assuming the boundary conditions (2.3), that

$$
\begin{aligned}
\frac{\mathrm{d}}{\mathrm{d}t} \, E_\lambda(\vec{x}) &= \frac{\mathrm{d}}{\mathrm{d}t} \int_I [G(|\vec{\varkappa}|) + \lambda] \, |\vec{x}_\rho| \, \mathrm{d}\rho \\
&= \int_I G'(|\vec{\varkappa}|) \, |\vec{\varkappa}|^{-1} \, \vec{\varkappa} \cdot \vec{\varkappa}_t \, |\vec{x}_\rho| \, \mathrm{d}\rho + \int_I [G(|\vec{\varkappa}|) + \lambda] \, (|\vec{x}_\rho|)_t \, \mathrm{d}\rho \\
&= -\int_I [G'(|\vec{\varkappa}|) \, |\vec{\varkappa}|^{-1} \, \vec{\varkappa}]_\rho \cdot \vec{\tau}_t \, \mathrm{d}\rho + \int_I \left[G(|\vec{\varkappa}|) - G'(|\vec{\varkappa}|) \, |\vec{\varkappa}| + \lambda \right] (|\vec{x}_\rho|)_t \, \mathrm{d}\rho \\
&= -\int_I \left(\underline{\underline{P}} \, [G'(|\vec{\varkappa}|) \, |\vec{\varkappa}|^{-1} \, \vec{\varkappa}]_s - [G(|\vec{\varkappa}|) - G'(|\vec{\varkappa}|) \, |\vec{\varkappa}| + \lambda] \, \vec{\tau} \right) \cdot (\vec{x}_t)_\rho \, \mathrm{d}\rho \\
&= \int_I \left(\underline{\underline{P}} \, [G'(|\vec{\varkappa}|) \, |\vec{\varkappa}|^{-1} \, \vec{\varkappa}]_s - [G(|\vec{\varkappa}|) - G'(|\vec{\varkappa}|) \, |\vec{\varkappa}| + \lambda] \, \vec{\tau} \right)_s \cdot \vec{x}_t \, |\vec{x}_\rho| \, \mathrm{d}\rho \,. \tag{2.12}
\end{aligned}
$$

Hence the strong form of the L^2–gradient flow of (2.5), subject to (2.3), is given by

$$\vec{x}_t = -\left(\underline{\underline{P}} \, [G'(|\vec{\varkappa}|) \, |\vec{\varkappa}|^{-1} \, \vec{\varkappa}]_s \right)_s + \left([G(|\vec{\varkappa}|) - G'(|\vec{\varkappa}|) \, |\vec{\varkappa}| + \lambda] \, \vec{\tau} \right)_s \,. \tag{2.13}$$

On noting from (2.9), $\vec{\tau}_s \cdot \vec{\tau} = 0$ and (2.4) that

$$
\begin{aligned}
\vec{\nabla}_s^2 \left(G'(|\vec{\varkappa}|) \, |\vec{\varkappa}|^{-1} \, \vec{\varkappa} \right) &= \left[\vec{\nabla}_s \left(G'(|\vec{\varkappa}|) \, |\vec{\varkappa}|^{-1} \, \vec{\varkappa} \right) \right]_s - \left(\left[\vec{\nabla}_s \left(G'(|\vec{\varkappa}|) \, |\vec{\varkappa}|^{-1} \, \vec{\varkappa} \right) \right]_s \cdot \vec{\tau} \right) \vec{\tau} \\
&= \left[\vec{\nabla}_s \left(G'(|\vec{\varkappa}|) \, |\vec{\varkappa}|^{-1} \, \vec{\varkappa} \right) \right]_s + \left[G'(|\vec{\varkappa}|) \, |\vec{\varkappa}|^{-1} \, \vec{\varkappa} \right]_s \cdot \vec{\tau}_s \, \vec{\tau} \\
&= \left[\vec{\nabla}_s \left(G'(|\vec{\varkappa}|) \, |\vec{\varkappa}|^{-1} \, \vec{\varkappa} \right) \right]_s + \left[G'(|\vec{\varkappa}|) \, |\vec{\varkappa}|^{-1} \right]_s |\vec{\varkappa}|^2 \, \vec{\tau} + G'(|\vec{\varkappa}|) \, |\vec{\varkappa}|^{-1} \, (\vec{\varkappa}_s \cdot \vec{\varkappa}) \, \vec{\tau} \\
&= \left[\vec{\nabla}_s \left(G'(|\vec{\varkappa}|) \, |\vec{\varkappa}|^{-1} \, \vec{\varkappa} \right) \right]_s + [G'(|\vec{\varkappa}|)]_s \, |\vec{\varkappa}| \, \vec{\tau} \,,
\end{aligned}
$$

we can rewrite (2.13) as

$$
\begin{aligned}
\vec{x}_t &= -\left[\vec{\nabla}_s [G'(|\vec{\varkappa}|) \, |\vec{\varkappa}|^{-1} \, \vec{\varkappa}] \right]_s + \left[G(|\vec{\varkappa}|) - G'(|\vec{\varkappa}|) \, |\vec{\varkappa}| \right]_s \vec{\tau} \\
&\qquad + \left[G(|\vec{\varkappa}|) - G'(|\vec{\varkappa}|) \, |\vec{\varkappa}| + \lambda \right] \vec{\varkappa} \\
&= -\vec{\nabla}_s^2 \left(G'(|\vec{\varkappa}|) \, |\vec{\varkappa}|^{-1} \, \vec{\varkappa} \right) + \left[G(|\vec{\varkappa}|) - G'(|\vec{\varkappa}|) \, |\vec{\varkappa}| + \lambda \right] \vec{\varkappa} \\
&\qquad + \left[G(|\vec{\varkappa}|) - G'(|\vec{\varkappa}|) \, |\vec{\varkappa}| \right]_s \vec{\tau} + [G'(|\vec{\varkappa}|)]_s \, |\vec{\varkappa}| \, \vec{\tau} \\
&= -\vec{\nabla}_s^2 \left(G'(|\vec{\varkappa}|) \, |\vec{\varkappa}|^{-1} \, \vec{\varkappa} \right) + \left[G(|\vec{\varkappa}|) - G'(|\vec{\varkappa}|) \, |\vec{\varkappa}| + \lambda \right] \vec{\varkappa} \\
&\qquad + \left([G(|\vec{\varkappa}|)]_s - G'(|\vec{\varkappa}|) \, [|\vec{\varkappa}|]_s \right) \vec{\tau} \\
&= -\vec{\nabla}_s^2 \left(G'(|\vec{\varkappa}|) \, |\vec{\varkappa}|^{-1} \, \vec{\varkappa} \right) + \left[G(|\vec{\varkappa}|) - G'(|\vec{\varkappa}|) \, |\vec{\varkappa}| + \lambda \right] \vec{\varkappa} \,. \tag{2.14}
\end{aligned}
$$

In case (1.3a) with $p = 2$ the above formulas (2.13) and (2.14) collapse to standard elastic flow

$$\vec{x}_t = -(\vec{\nabla}_s \vec{\varkappa})_s - \tfrac{1}{2} \left(|\vec{\varkappa}|^2 \, \vec{\tau} \right)_s + \lambda \, \vec{\varkappa} = -\vec{\nabla}_s^2 \vec{\varkappa} - \tfrac{1}{2} \, |\vec{\varkappa}|^2 \, \vec{\varkappa} + \lambda \, \vec{\varkappa} \,, \tag{2.15}$$

5

see also Barrett *et al.* (2010, (2.25))). As the right hand side in (2.14) is normal to the curve, an alternative formulation of (2.13) is given by

$$\underline{\underline{P}}\,\vec{x}_t = -\left(\underline{\underline{P}}\,[G'(|\vec{\varkappa}|)\,|\vec{\varkappa}|^{-1}\,\vec{\varkappa}]_s\right)_s + \left([G(|\vec{\varkappa}|) - G'(|\vec{\varkappa}|)\,|\vec{\varkappa}| + \lambda]\,\vec{\tau}\right)_s. \qquad (2.16)$$

3 Weak formulations

We define the first variation of a quantity A depending on $\vec{x}$, in the direction $\vec{\chi}$ as

$$\left[\frac{\delta}{\delta\vec{x}}\,A(\vec{x})\right](\vec{\chi}) = \lim_{\varepsilon\to 0}\frac{A(\vec{x}+\varepsilon\,\vec{\chi}) - A(\vec{x})}{\varepsilon}\,. \qquad (3.1)$$

For later use, on noting (3.1) and (2.2), we observe that

$$\left[\frac{\delta}{\delta\vec{x}}\,|\vec{x}_\rho|\right](\vec{\chi}) = \frac{\vec{x}_\rho\cdot\vec{\chi}_\rho}{|\vec{x}_\rho|} = \vec{\tau}\cdot\vec{\chi}_\rho\,, \qquad (3.2\text{a})$$

$$\left[\frac{\delta}{\delta\vec{x}}\,\vec{\tau}\right](\vec{\chi}) = \left[\frac{\delta}{\delta\vec{x}}\,\frac{\vec{x}_\rho}{|\vec{x}_\rho|}\right](\vec{\chi}) = \frac{1}{|\vec{x}_\rho|}\,\underline{\underline{P}}\,\vec{\chi}_\rho = \underline{\underline{P}}\,\vec{\chi}_s\,, \qquad (3.2\text{b})$$

$$\left[\frac{\delta}{\delta\vec{x}}\,\vec{x}_\rho\right](\vec{\chi}) = \vec{\chi}_\rho\,, \qquad (3.2\text{c})$$

where we always assume that $\vec{\chi}$ is sufficiently smooth so that all the quantities are defined almost everywhere; e.g. $\vec{\chi}\in[W^{1,\infty}(I)]^d$. In addition, we note that

$$\left[\frac{\delta}{\delta\vec{x}}\,A(\vec{x})\right](\vec{x}_t) = \frac{\mathrm{d}}{\mathrm{d}t}\,A(\vec{x})\,. \qquad (3.3)$$

For example, (2.12) can be read as $[\delta/\delta\vec{x}\,E_\lambda(\vec{x})](\vec{x}_t)$.

3.1 Weak formulation without tangential motion

The differential equations obtained in the previous section are first order in time but fourth order in space. It is in view of numerical methods more convenient to write the equations in $\vec{x}$ and $\vec{\varkappa}$, but coupled by (2.4), since it allows to use first order methods. The weak formulation will then be derived from the corresponding Lagrange function. For convenience we will denote by $(\cdot,\cdot)$ the L^2–inner product on I.

Weak formulation. Given $\Gamma(0) = \vec{x}(I, 0)$, with $\vec{x}(0) \in \underline{V}$ for all $t \in (0, T]$, find $\Gamma(t) = \vec{x}(I, t)$, where $\vec{x}_t(t) \in \underline{W}$, $\vec{\varkappa}(t) \in \underline{V}$ and $\vec{y}(t) \in \underline{V}$, such that

$$\left(\vec{x}_t, \vec{\chi} \, |\vec{x}_\rho|\right) - \left(\underline{P} \, \vec{y}_s, \vec{\chi}_\rho\right)$$
$$+ \left(G(|\vec{\varkappa}|) + \lambda - \vec{\varkappa} \cdot \vec{y}, \vec{\chi}_\rho \cdot \vec{\tau}\right) = 0 \qquad\qquad \forall \, \vec{\chi} \in \underline{W} \,. \tag{3.4a}$$

$$\left(G'(|\vec{\varkappa}|) \, |\vec{\varkappa}|^{-1} \, \vec{\varkappa} - \vec{y}, \vec{\xi} \, |\vec{x}_\rho|\right) = 0 \qquad\qquad \forall \, \vec{\xi} \in [L^2(I)]^d \,, \tag{3.4b}$$

$$\left(\vec{\varkappa}, \vec{\eta} \, |\vec{x}_\rho|\right) + \left(\vec{\tau}, \vec{\eta}_\rho\right) = \sum_{q \in \partial I} \vec{\zeta}_q \cdot \vec{\eta}(q) \qquad \forall \, \vec{\eta} \in \underline{V} \,. \tag{3.4c}$$

Lagrange formalism. We derive the weak equations by using the formal calculus of PDE constrained optimisation, see e.g. Tröltzsch (2010). For our constrained problem we define the Lagrangian

$$\mathcal{L}_1(\vec{x}, \vec{\varkappa}, \vec{y}) = \left(G(|\vec{\varkappa}|) + \lambda, |\vec{x}_\rho|\right) - \left(\vec{\varkappa}, \vec{y} \, |\vec{x}_\rho|\right) - \left(\vec{\tau}, \vec{y}_\rho\right) + \sum_{q \in \partial I} \vec{\zeta}_q \cdot \vec{y}(q) \,,$$

i.e. we consider the gradient flow of (2.5) subject to the constraint (2.10). Taking variations $\vec{\chi} \in \underline{W}$ in $\vec{x}$, and setting $\left(\vec{x}_t, \vec{\chi} \, |\vec{x}_\rho|\right) + \left[\frac{\delta}{\delta \vec{x}} \mathcal{L}_1\right](\vec{\chi}) = 0$ we obtain that

$$\left(\vec{x}_t, \vec{\chi} \, |\vec{x}_\rho|\right) + \left(G(|\vec{\varkappa}|) + \lambda - \vec{\varkappa} \cdot \vec{y}, \left[\frac{\delta}{\delta \vec{x}} |\vec{x}_\rho|\right](\vec{\chi})\right) - \left(\vec{y}_\rho, \left[\frac{\delta}{\delta \vec{x}} \vec{\tau}\right](\vec{\chi})\right) = 0 \qquad \forall \, \vec{\chi} \in \underline{W} \,. \tag{3.5}$$

On recalling (3.2a,b), it follows from (3.5) that

$$\left(\vec{x}_t, \vec{\chi} \, |\vec{x}_\rho|\right) - \left(\underline{P} \, \vec{y}_s, \vec{\chi}_\rho\right) + \left(G(|\vec{\varkappa}|) + \lambda - \vec{\varkappa} \cdot \vec{y}, \vec{\chi}_\rho \cdot \vec{\tau}\right) = 0 \qquad \forall \, \vec{\chi} \in \underline{W}$$

and thus (3.4a). Taking now variations $[\frac{\delta}{\delta \vec{\varkappa}} \mathcal{L}_1](\vec{\xi})$ and $[\frac{\delta}{\delta \vec{y}} \mathcal{L}_1](\vec{\eta})$, for $\vec{\xi} \in [L^2(I)]^d$ and $\vec{\eta} \in \underline{V}$, and setting them to zero yields (3.4b) and (3.4c).

Stability. It follows from (3.4b) that

$$\vec{y} = G'(|\vec{\varkappa}|) \, |\vec{\varkappa}|^{-1} \, \vec{\varkappa} \,. \tag{3.6}$$

Then the weak form (3.4) reduces to

$$\left(\vec{x}_t, \vec{\chi} \, |\vec{x}_\rho|\right) - \left(\underline{P} \, [G'(|\vec{\varkappa}|) \, |\vec{\varkappa}|^{-1} \, \vec{\varkappa}]_s, \vec{\chi}_\rho\right)$$
$$+ \left([G(|\vec{\varkappa}|) - G'(|\vec{\varkappa}|) \, |\vec{\varkappa}| + \lambda] \, \vec{\tau}, \vec{\chi}_\rho\right) = 0 \qquad\qquad \forall \, \vec{\chi} \in \underline{W} \,, \tag{3.7a}$$

$$\left(\vec{\varkappa}, \vec{\eta} \, |\vec{x}_\rho|\right) + \left(\vec{\tau}, \vec{\eta}_\rho\right) = \sum_{q \in \partial I} \vec{\zeta}_q \cdot \vec{\eta}(q) \qquad \forall \, \vec{\eta} \in \underline{V} \,. \tag{3.7b}$$

Choosing $\vec{\chi} = \vec{x}_t \in \underline{W}$ in (3.7a), on recalling (2.12), yields that

$$\frac{\mathrm{d}}{\mathrm{d}t} \, E_\lambda(\vec{x}) + \left(|\vec{x}_t|^2, |\vec{x}_\rho|\right) = 0 \,, \tag{3.8}$$

7

and thus provides the stability result $\frac{\mathrm{d}}{\mathrm{d}t} E_\lambda(\vec{x}) \leq 0$.

We remark that in an alternative to the Lagrange formalism above, the weak formulation (3.7) can also be obtained directly by testing (2.13) with functions in $\underline{W}$ and using (2.10). We note that in case (1.3a) with $p = 2$, (3.7) collapses to the weak formulation of Deckelnick and Dziuk (2009, (2.2), (2.3)) for elastic flow.

3.2 Weak formulation with tangential motion

In the following, based on the techniques in Barrett *et al.* (2012), we will introduce an alternative weak formulation for the L^2–gradient flow of the energy (2.5), by imposing the two constraints

$$\left(\vec{\varkappa}, \vec{\eta} \,|\vec{x}_\rho|\right) + \left(\vec{\tau}, \vec{\eta}_\rho\right) = \sum_{q \in \partial I} \vec{\zeta}_q \cdot \vec{\eta}(q) \qquad \forall \, \vec{\eta} \in \underline{V} \tag{3.9a}$$

and
$$\left(\vec{\varkappa} \cdot \vec{\tau}, \chi \,|\vec{x}_\rho|\right) = 0 \qquad \forall \, \chi \in L^2(I) \,. \tag{3.9b}$$

We recall that the right hand side in (3.9a) is zero in the case $I = \mathbb{R}/\mathbb{Z}$. Here we should stress that the finite element discretisation of the constraints (3.9), building on the ideas published in Barrett *et al.* (2012), will lead to an induced tangential motion that gives rise to an equidistribution property in the semidiscrete setting, Section 4. Of course, on the continuous level the constraint (3.9b) is redundant, recall (2.4) and (2.1). We will formally establish that solutions to this weak formulation are indeed solutions to the L^2–gradient flow of (2.5). Mimicking this stability proof on the discrete level will yield the main result Theorem 2 of this paper.

Weak formulation. Given $\Gamma(0) = \vec{x}(I, 0)$, with $\vec{x}(0) \in \underline{V}$, for all $t \in (0, T]$ find $\Gamma(t) = \vec{x}(I, t)$, where $\vec{x}_t(t) \in \underline{W}$, $\vec{\varkappa}(t) \in \underline{V}$ and $\vec{y}(t) \in \underline{V}$ such that

$$\left(\underline{P} \, \vec{x}_t, \vec{\chi} \,|\vec{x}_\rho|\right) - \left(\underline{P} \, \vec{y}_s, \vec{\chi}_\rho\right)$$
$$+ \left([G(|\vec{\varkappa}|) + \lambda - \vec{\varkappa} \cdot \vec{y}] \, \vec{\tau} + (\vec{y} \cdot \vec{\tau}) \, \vec{\varkappa}, \vec{\chi}_\rho\right) = 0 \qquad \forall \, \vec{\chi} \in \underline{W} \,, \tag{3.10a}$$
$$\left(G'(|\vec{\varkappa}|) \, |\vec{\varkappa}|^{-1} \, \vec{\varkappa} - \underline{P} \, \vec{y}, \vec{\xi} \,|\vec{x}_\rho|\right) = 0 \qquad \forall \, \vec{\xi} \in [L^2(I)]^d \,, \tag{3.10b}$$
$$\left(\vec{\varkappa}, \vec{\eta} \,|\vec{x}_\rho|\right) + \left(\vec{\tau}, \vec{\eta}_\rho\right) = \sum_{q \in \partial I} \vec{\zeta}_q \cdot \vec{\eta}(q) \qquad \forall \, \vec{\eta} \in \underline{V} \,. \tag{3.10c}$$

We observe that in the case (1.3a) with $p = 2$, the formulation (3.10), for $I = \mathbb{R}/\mathbb{Z}$, collapses to Barrett *et al.* (2012, (2.4)) on noting that then (3.10b) implies that $\vec{\varkappa} = \underline{P} \, \vec{y}$. It is straightforward to show that sufficiently smooth solutions to (3.10) satisfy (2.16), i.e. that the weak formulation (3.10) is consistent with (2.16).

8

Lagrange formalism. We introduce Lagrange multipliers $\vec{y} \in \underline{V}$ and $z \in L^2(I)$ for (3.9), and define the Lagrangian

$$\mathcal{L}_2(\vec{x}, \vec{\varkappa}, \vec{y}, z) = (G(|\vec{\varkappa}|) + \lambda, |\vec{x}_\rho|) - (\vec{\varkappa}, \vec{y}\,|\vec{x}_\rho|) - (\vec{\tau}, \vec{y}_\rho) + \sum_{q \in \partial I} \vec{\zeta}_q \cdot \vec{y}(q)$$
$$+ (\vec{\varkappa} \cdot \vec{x}_\rho, z)\,.$$

We start by taking variations $[\frac{\delta}{\delta \vec{y}}\mathcal{L}_2](\vec{\eta})$, $[\frac{\delta}{\delta \vec{\varkappa}}\mathcal{L}_2](\vec{\xi})$, $[\frac{\delta}{\delta z}\mathcal{L}_2](\chi)$ and setting them to zero. While the first term immediately yields (3.10c), the remaining equations are

$$\left(G'(|\vec{\varkappa}|)\,|\vec{\varkappa}|^{-1}\,\vec{\varkappa} - \vec{y} + z\,\vec{\tau}, \vec{\xi}\,|\vec{x}_\rho| \right) = 0 \qquad \forall\, \vec{\xi} \in [L^2(I)]^d\,, \tag{3.11a}$$

$$(\vec{\varkappa} \cdot \vec{x}_\rho, \chi) = 0 \qquad \forall\, \chi \in L^2(I)\,. \tag{3.11b}$$

Taking variations $\vec{\chi} \in \underline{W}$ in $\vec{x}$, and setting $(\underline{\underline{P}}\,\vec{x}_t, \vec{\chi}\,|\vec{x}_\rho|) + \left[\frac{\delta}{\delta \vec{x}}\mathcal{L}_2\right](\vec{\chi}) = 0$ yields that

$$\left(\underline{\underline{P}}\,\vec{x}_t, \vec{\chi}\,|\vec{x}_\rho|\right) + \left(G(|\vec{\varkappa}|) + \lambda - \vec{\varkappa} \cdot \vec{y}, \left[\frac{\delta}{\delta \vec{x}}\,|\vec{x}_\rho|\right](\vec{\chi}) \right)$$
$$- \left(\vec{y}_\rho, \left[\frac{\delta}{\delta \vec{x}}\,\vec{\tau}\right](\vec{\chi}) \right) + \left(z\,\vec{\varkappa}, \left[\frac{\delta}{\delta \vec{x}}\,\vec{x}_\rho\right](\vec{\chi}) \right) = 0 \qquad \forall\, \vec{\chi} \in \underline{W}\,. \tag{3.12}$$

On recalling (3.2), it follows from (3.12) that

$$\left(\underline{\underline{P}}\,\vec{x}_t, \vec{\chi}\,|\vec{x}_\rho|\right) + \left(G(|\vec{\varkappa}|) + \lambda - \vec{\varkappa} \cdot \vec{y}, \vec{\tau} \cdot \vec{\chi}_\rho \right) - \left(\vec{y}_\rho, \underline{\underline{P}}\,\vec{\chi}_s\right) + \left(z\,\vec{\varkappa}, \vec{\chi}_\rho \right) = 0 \quad \forall\, \vec{\chi} \in \underline{W}\,. \tag{3.13}$$

In addition, it follows from (3.11a,b) by considering the normal and tangential part that

$$\underline{\underline{P}}\,\vec{y} = G'(|\vec{\varkappa}|)\,|\vec{\varkappa}|^{-1}\,\vec{\varkappa} \quad \text{and} \quad z = \vec{y} \cdot \vec{\tau}\,. \tag{3.14}$$

With the first term we can provide (3.10b), while inserting the second identity into (3.13) gives (3.10a).

Stability. Choosing $\vec{\chi} = \vec{x}_t \in \underline{W}$ in (3.12), and noting (3.3), yields that

$$\left(|\underline{\underline{P}}\,\vec{x}_t|^2, |\vec{x}_\rho|\right) + (G(|\vec{\varkappa}|) + \lambda - \vec{\varkappa} \cdot \vec{y}, (|\vec{x}_\rho|)_t) - (\vec{y}_\rho, \vec{\tau}_t) + (z\,\vec{\varkappa}, \vec{x}_{\rho,t}) = 0\,. \tag{3.15}$$

Differentiating (3.10c) with respect to time, and then choosing $\vec{\eta} = \vec{y}$ yields

$$(\vec{\varkappa}_t, \vec{y}\,|\vec{x}_\rho|) + (\vec{\varkappa} \cdot \vec{y}, (|\vec{x}_\rho|)_t) + (\vec{y}_\rho, \vec{\tau}_t) = 0\,. \tag{3.16}$$

Differentiating (3.9b) with respect to t, and then choosing $\chi = z$ yields that

$$(z\,\vec{\varkappa}_t, \vec{x}_\rho) + (z\,\vec{\varkappa}, \vec{x}_{t,\rho}) = 0\,. \tag{3.17}$$

Choosing $\vec{\zeta} = \vec{\varkappa}_t$ in (3.11a) yields that

$$(\vec{y} - z\,\vec{\tau}, \vec{\varkappa}_t\,|\vec{x}_\rho|) = \left(G'(|\vec{\varkappa}|)\,|\vec{\varkappa}|^{-1}\,\vec{\varkappa}, \vec{\varkappa}_t\,|\vec{x}_\rho| \right) = ([G(|\vec{\varkappa}|)]_t\,, |\vec{x}_\rho|)\,. \tag{3.18}$$

Combining (3.15), (3.16), (3.17) and (3.18) yields that

$$
\begin{aligned}
\frac{\mathrm{d}}{\mathrm{d}t}\, E_\lambda(\vec{x}, \vec{\varkappa}) &= \frac{\mathrm{d}}{\mathrm{d}t}\, (G(|\vec{\varkappa}|), |\vec{x}_\rho|) + (\lambda, (|\vec{x}_\rho|)_t) \\
&= ([G(|\vec{\varkappa}|)]_t, |\vec{x}_\rho|) + (G(|\vec{\varkappa}|) + \lambda, (|\vec{x}_\rho|)_t) \\
&= (\vec{y} - z\,\vec{\tau}, \vec{\varkappa}_t\, |\vec{x}_\rho|) + (G(|\vec{\varkappa}|) + \lambda, (|\vec{x}_\rho|)_t) \\
&= (G(|\vec{\varkappa}|) + \lambda - \vec{\varkappa} \cdot \vec{y}, (|\vec{x}_\rho|)_t) - (\vec{y}_\rho, \vec{\tau}_t) + (z\, \vec{\varkappa}, \vec{x}_{t,\rho}) \\
&= -\left(|\underline{P}\, \vec{x}_t|^2, |\vec{x}_\rho|\right) \le 0\,,
\end{aligned} \tag{3.19}
$$

which shows that (3.10) is indeed a weak formulation of the L^2–gradient flow of (2.5).

4 Semidiscrete in space finite element approximation

Let $[0,1] = \cup_{j=1}^J I_j$, $J \ge 3$, be a decomposition of $[0,1]$ into intervals $I_j = [q_{j-1}, q_j]$ given by a set of nodes q_j. For simplicity, and without loss of generality, we assume that the subintervals form an equipartitioning of $[0,1]$, i.e. that

$$
q_j = j\,h\,, \quad \text{with} \quad h = J^{-1}\,, \qquad j = 0, \ldots, J\,. \tag{4.1}
$$

In case $I = \mathbb{R}/\mathbb{Z}$ we identify $0 = q_0 = q_J = 1$, and set $q_{J+1} = q_1$.

The finite element spaces we use are given as follows:

$$
V^h = \{\chi \in C(\overline{I}) : \chi|_{I_j} \text{ is linear } \forall\, j = 1, \ldots, J\} \quad \text{and} \quad \underline{V}^h = [V^h]^d\,.
$$

Let $\{\chi_j\}_{j=j_0}^J$ denote the standard basis of V^h, where $j_0 = 0$ if $I = (0,1)$ and $j_0 = 1$ if $I = \mathbb{R}/\mathbb{Z}$. We also set $j_1 = J - 1$ if $I = (0,1)$ and $j_1 = J$ if $I = \mathbb{R}/\mathbb{Z}$. Let $\pi^h : C(\overline{I}) \to V^h$ be the standard interpolation operator at the nodes $\{q_j\}_{j=0}^J$, and similarly for $\vec{\pi}^h : [C(I)]^d \to \underline{V}^h$. Moreover, we define the spaces

$$
W^h = V^h \cap H_0^1(I) \quad \text{and} \quad \underline{W}^h = [W^h]^d\,. \tag{4.2}
$$

Let $\pi_W^h : C(\overline{I}) \to W^h$ be the standard Lagrange interpolation operator with zero Dirichlet boundary conditions.

Similarly to $(\cdot, \cdot)$, the L^2–inner product on I, we define the mass-lumped L^2–inner product $(\cdot, \cdot)^h$, for two piecewise continuous functions u, v, with possible jumps at the nodes $\{q_j\}_{j=1}^{J-1}$, via

$$
(u, v)^h = \tfrac{1}{2}\, h \sum_{j=1}^J \left[(u\,v)(q_j^-) + (u\,v)(q_{j-1}^+)\right], \tag{4.3}
$$

where we define $u(q_j^\pm) = \lim_{\delta \searrow 0} u(q_j \pm \delta)$. The definition (4.3) naturally extends to vector valued functions.

Let $\vec{X}^h : [0, T] \to \underline{V}^h$ be an approximation to $\vec{x} : [0, T] \to \underline{V}$. Here we make the quite natural assumption that

$(\mathcal{C}_1^h)$ $\vec{X}^h(q_j, t) \neq \vec{X}^h(q_{j+1}, t)$, $j = 0, \ldots, J - 1$, for all $t \in [0, T]$.

Then, in correspondence to (2.2) and (2.9), we set

$$\vec{\tau}^h = \vec{X}_s^h = \frac{\vec{X}_\rho^h}{|\vec{X}_\rho^h|} \quad \text{and} \quad \underline{\underline{P}}^h = \underline{\underline{\mathrm{Id}}} - \vec{\tau}^h \otimes \vec{\tau}^h. \tag{4.4}$$

Moreover, in analogy to (3.2), on noting (3.1) and (4.4), we have for all $\vec{\chi} \in \underline{V}^h$ on I_j, $j = 1, \ldots, J$, that

$$\left[\frac{\delta}{\delta \vec{X}^h} |\vec{X}_\rho^h| \right] (\vec{\chi}) = \frac{\vec{X}_\rho^h \cdot \vec{\chi}_\rho}{|\vec{X}_\rho^h|} = \vec{\tau}^h \cdot \vec{\chi}_\rho, \tag{4.5a}$$

$$\left[\frac{\delta}{\delta \vec{X}^h} \vec{\tau}^h \right] (\vec{\chi}) = \left[\frac{\delta}{\delta \vec{X}^h} \frac{\vec{X}_\rho^h}{|\vec{X}_\rho^h|} \right] (\vec{\chi}) = \frac{1}{|\vec{X}_\rho^h|} \underline{\underline{P}}^h \vec{\chi}_\rho = \underline{\underline{P}}^h \vec{\chi}_s, \tag{4.5b}$$

$$\left[\frac{\delta}{\delta \vec{X}^h} \vec{X}_\rho^h \right] (\vec{\chi}) = \vec{\chi}_\rho. \tag{4.5c}$$

Given $\vec{X}^h, \vec{\kappa}^h \in \underline{V}^h$, we define the discrete energy

$$E_\lambda^h(\vec{X}^h, \vec{\kappa}^h) = \left(G(|\vec{\kappa}^h|) + \lambda, |\vec{X}_\rho^h| \right)^h. \tag{4.6}$$

4.1 Semidiscrete method without tangential motion

We consider the following semidiscrete continuous-in-time finite element approximation of (3.4).

Semidiscrete weak formulation. Let $\vec{X}^h(0) \in \underline{V}^h$. For $t \in (0, T]$ find $\vec{X}^h(t)$, $\vec{\kappa}^h(t)$, $\vec{Y}^h(t) \in \underline{V}^h$, with $\vec{X}_t^h(t) \in \underline{W}^h$, such that

$$\left(\vec{X}_t^h, \vec{\chi} \, |\vec{X}_\rho^h| \right)^h - \left(\underline{\underline{P}}^h \vec{Y}_s^h, \vec{\chi}_s \, |\vec{X}_\rho^h| \right)$$

$$+ \left([G(|\vec{\kappa}^h|) + \lambda - \vec{\kappa}^h \cdot \vec{Y}^h] \, \vec{X}_s^h, \vec{\chi}_s \, |\vec{X}_\rho^h| \right)^h = 0 \qquad \forall \, \vec{\chi} \in \underline{W}^h, \tag{4.7a}$$

$$\left(G'(|\vec{\kappa}^h|) \, |\vec{\kappa}^h|^{-1} \vec{\kappa}^h - \vec{Y}^h, \vec{\xi} \, |\vec{X}_\rho^h| \right)^h = 0 \qquad \forall \, \vec{\xi} \in \underline{V}^h, \tag{4.7b}$$

$$\left(\vec{\kappa}^h, \vec{\eta} \, |\vec{X}_\rho^h| \right)^h + \left(\vec{X}_s^h, \vec{\eta}_s \, |\vec{X}_\rho^h| \right) = \sum_{q \in \partial I} \vec{\zeta}_q \cdot \vec{\eta}(q) \qquad \forall \, \vec{\eta} \in \underline{V}^h. \tag{4.7c}$$

In case (1.3a) with $p = 2$, it follows from (4.7b) that $\vec{\kappa}^h = \vec{Y}^h$, and so the scheme (4.7), for the case $I = \mathbb{R}/\mathbb{Z}$, collapses to the scheme (2.9), (2.10) in Deckelnick and Dziuk (2009) for elastic flow of closed curves in $\mathbb{R}^d$.

11

Semidiscrete Lagrange formalism. On recalling (4.6), and with a view to the constraint (4.7c), we define the discrete Lagrangian

$$\mathcal{L}_1^h(\vec{X}^h, \vec{\kappa}^h, \vec{Y}^h) = \left(G(|\vec{\kappa}^h|) + \lambda, |\vec{X}_\rho^h| \right)^h - \left(\vec{\kappa}^h, \vec{Y}^h |\vec{X}_\rho^h| \right)^h - \left(\vec{\tau}^h, \vec{Y}_\rho^h \right) + \sum_{q \in \partial I} \vec{\zeta}_q \cdot \vec{Y}^h(q) , \quad (4.8)$$

where $\vec{Y}^h \in \underline{V}^h$ is a Lagrange multiplier for (4.7c). Taking variations $[\frac{\delta}{\delta \vec{\kappa}^h} \mathcal{L}_1^h](\vec{\xi})$ and $[\frac{\delta}{\delta \vec{Y}^h} \mathcal{L}_1^h](\vec{\eta})$, for $\vec{\xi}, \vec{\eta} \in \underline{V}^h$, and setting them to zero yields immediately (4.7b) and (4.7c). Taking variations $\vec{\chi} \in \underline{W}^h$ in $\vec{X}^h$, and setting $(\vec{X}_t^h, \vec{\chi} |\vec{X}_\rho^h|)^h + \left[\frac{\delta}{\delta \vec{x}} \mathcal{L}_1^h \right](\vec{\chi}) = 0$ we obtain with (4.5a) that

$$\left(\vec{X}_t^h, \vec{\chi} |\vec{X}_\rho^h| \right)^h + \left(G(|\vec{\kappa}^h|) + \lambda - \vec{\kappa}^h \cdot \vec{Y}^h, \vec{\tau}^h \cdot \vec{\chi}_\rho \right)^h - \left(\vec{Y}_\rho^h, \underline{\underline{P}}^h \vec{\chi}_s \right) = 0 \quad \forall \vec{\chi} \in \underline{W}^h , \quad (4.9)$$

which is equivalent to (4.7a).

Stability. Choosing $\vec{\chi} = \vec{X}_t^h \in \underline{W}^h$ in (4.9), and noting (3.3), yields that

$$\left(|\vec{X}_t^h|^2, |\vec{X}_\rho^h| \right)^h + \left(G(|\vec{\kappa}^h|) + \lambda - \vec{\kappa}^h \cdot \vec{Y}^h, (|\vec{X}_\rho^h|)_t \right)^h - \left(\vec{Y}_\rho^h, \vec{\tau}_t^h \right) = 0 . \quad (4.10)$$

Differentiating (4.7c) with respect to time, and then choosing $\vec{\eta} = \vec{Y}^h$ yields that

$$\left(\vec{\kappa}_t^h, \vec{Y}^h |\vec{X}_\rho^h| \right)^h + \left(\vec{\kappa}^h \cdot \vec{Y}^h, (|\vec{X}_\rho^h|)_t \right)^h + \left(\vec{Y}_\rho^h, \vec{\tau}_t^h \right) = 0 . \quad (4.11)$$

Choosing $\vec{\zeta} = \vec{\kappa}_t^h$ in (4.7b) yields that

$$\left(\vec{Y}^h, \vec{\kappa}_t^h |\vec{X}_\rho^h| \right)^h = \left(G'(|\vec{\kappa}^h|) |\vec{\kappa}^h|^{-1} \vec{\kappa}^h, \vec{\kappa}_t^h |\vec{X}_\rho^h| \right)^h = \left([G(|\vec{\kappa}^h|)]_t, |\vec{X}_\rho^h| \right)^h . \quad (4.12)$$

Combining (4.10), (4.11) and (4.12) yields that

$$\begin{aligned}
\frac{d}{dt} E_\lambda^h(\vec{X}^h, \vec{\kappa}^h) &= \frac{d}{dt} \left(G(|\vec{\kappa}^h|), |\vec{X}_\rho^h| \right)^h + \left(\lambda, (|\vec{X}_\rho^h|)_t \right)^h \\
&= \left([G(|\vec{\kappa}^h|)]_t, |\vec{X}_\rho^h| \right)^h + \left(G(|\vec{\kappa}^h|) + \lambda, (|\vec{X}_\rho^h|)_t \right)^h \\
&= - \left(|\vec{X}_t^h|^2, |\vec{X}_\rho^h| \right)^h \le 0 ,
\end{aligned} \quad (4.13)$$

and so a solution satisfying (4.7) is stable. In fact, we have shown the following result.

THEOREM 1. *Let* $G \in C^1(\mathbb{R}_{\ge 0}, \mathbb{R}_{>0})$ *satisfy* (2.6). *Let* $(\vec{X}^h(t), \vec{\kappa}^h(t), \vec{Y}^h(t))_{t \in (0, T]}$ *denote a solution to* (4.7), *with* $(\vec{X}^h(t))_{t \in (0, T]}$ *satisfying* $(\mathcal{C}_1^h)$. *Then it holds that*

$$\frac{d}{dt} E_\lambda^h(\vec{X}^h, \vec{\kappa}^h) + \left(|\vec{X}_t^h|^2, |\vec{X}_\rho^h| \right)^h = 0 .$$

12

4.2 Semidiscrete method with tangential motion

We now derive a semidiscrete formulation for (3.10). For this we need a few more definitions. Here we make the mild assumption that

$(\mathcal{C}_2^h)$ Let $(\mathcal{C}_1^h)$ hold and let $\vec{X}^h(q_{j-1},t) \neq \vec{X}^h(q_{j+1},t)$, $j = 1,\ldots,j_1$, for all $t \in [0,T]$.

Let $\vec{\theta}^h \in \underline{V}^h$ be the mass-lumped L^2–projection of $\vec{\tau}^h$ onto $\underline{V}^h$, i.e.

$$\left(\vec{\theta}^h, \vec{\varphi}\,|\vec{X}_\rho^h|\right)^h = \left(\vec{\tau}^h, \vec{\varphi}\,|\vec{X}_\rho^h|\right) = \left(\vec{\tau}^h, \vec{\varphi}\,|\vec{X}_\rho^h|\right)^h \qquad \forall\,\vec{\varphi} \in \underline{V}^h. \tag{4.14}$$

Following the notation in Barrett *et al.* (2012, (3.3)), we then define $\vec{\omega}_d^h(t) \in \underline{V}^h$ to be

$$\vec{\omega}_d^h(t) = \frac{\vec{\theta}^h(t)}{|\vec{\theta}^h(t)|}, \tag{4.15}$$

which, on noting assumption $(\mathcal{C}_2^h)$, is well-defined. Let

$$\underline{\underline{Q}}^h(\rho,t) = \underline{\underline{\mathrm{Id}}} - \vec{\omega}_d^h(\rho,t) \otimes \vec{\omega}_d^h(\rho,t), \qquad \forall\,\rho \in [0,1],\forall\,t \in [0,T], \tag{4.16}$$

and introduce the modified operator

$$\underline{\underline{Q}}_\star^h(\rho,t) = \begin{cases} \underline{\underline{Q}}^h(\rho,t) & \forall\,\rho \in I, \\ \underline{\underline{\mathrm{Id}}} & \forall\,\rho \in \partial I. \end{cases} \tag{4.17}$$

Semidiscrete weak formulation. Let $\vec{X}^h(0) \in \underline{V}^h$. For $t \in (0,T]$ find $\vec{X}^h(t)$, $\vec{\kappa}^h(t)$, $\vec{Y}^h(t) \in \underline{V}^h$, with $\vec{X}_t^h(t) \in \underline{W}^h$, such that

$$\left(\underline{\underline{Q}}^h\,\vec{X}_t^h, \vec{\chi}\,|\vec{X}_\rho^h|\right)^h - \left(\underline{\underline{P}}^h\,\vec{Y}_s^h, \vec{\chi}_s\,|\vec{X}_\rho^h|\right)$$

$$= -\left([G(|\vec{\kappa}^h|) + \lambda - \vec{\kappa}^h \cdot \vec{Y}^h]\,\vec{X}_s^h, \vec{\chi}_s\,|\vec{X}_\rho^h|\right)^h$$

$$- \left(\pi_W^h\,[|\vec{\theta}^h|^{-1}\,(\vec{Y}^h \cdot \vec{\omega}_d^h)]\,\vec{\kappa}^h, \vec{\chi}_s\,|\vec{X}_\rho^h|\right)^h \qquad \forall\,\vec{\chi} \in \underline{W}^h, \quad (4.18a)$$

$$\left(G'(|\vec{\kappa}^h|)\,|\vec{\kappa}^h|^{-1}\,\vec{\kappa}^h - \underline{\underline{Q}}_\star^h\,\vec{Y}^h, \vec{\xi}\,|\vec{X}_\rho^h|\right)^h = 0 \qquad \forall\,\vec{\xi} \in \underline{V}^h, \quad (4.18b)$$

$$\left(\vec{\kappa}^h, \vec{\eta}\,|\vec{X}_\rho^h|\right)^h + \left(\vec{X}_s^h, \vec{\eta}_s\,|\vec{X}_\rho^h|\right) = \sum_{q \in \partial I} \vec{\zeta}_q \cdot \vec{\eta}(q) \quad \forall\,\vec{\eta} \in \underline{V}^h. \quad (4.18c)$$

Discrete Lagrangian. We consider the L^2–gradient flow of the discrete energy (4.6), subject to the constraints

$$\left(\vec{\kappa}^h, \vec{\eta}\,|\vec{X}_\rho^h|\right)^h + \left(\vec{X}_s^h, \vec{\eta}_s\,|\vec{X}_\rho^h|\right) = \sum_{q \in \partial I} \vec{\zeta}_q \cdot \vec{\eta}(q) \qquad \forall\,\vec{\eta} \in \underline{V}^h \tag{4.19a}$$

and

$$\left(\vec{\kappa}^h \cdot \vec{X}_\rho^h, \chi\right)^h = 0 \qquad \forall\,\chi \in W^h. \tag{4.19b}$$

13

To this end, we define the discrete Lagrangian

$$\mathcal{L}_2^h(\vec{X}^h, \vec{\kappa}^h, \vec{Y}^h, Z^h) = \left(G(|\vec{\kappa}^h|) + \lambda, |\vec{X}_\rho^h| \right)^h - \left(\vec{\kappa}^h, \vec{Y}^h | \vec{X}_\rho^h | \right)^h - \left(\vec{\tau}^h, \vec{Y}_\rho^h \right)$$
$$+ \sum_{q \in \partial I} \vec{\zeta}_q \cdot \vec{Y}^h(q) + \left(\vec{\kappa}^h \cdot \vec{X}_\rho^h, Z^h \right)^h , \tag{4.20}$$

where $\vec{Y}^h \in \underline{V}^h$ and $Z^h \in W^h$ are Lagrange multipliers for (4.19a) and (4.19b), respectively. Here the test space W^h in (4.19b) was chosen because it is sufficient to obtain the desired equidistribution result, and this leads to the altered projection $\underline{\underline{Q}}_\star^h$ in (4.18b). For the choice (1.3a) with $p = 2$, the same strategy was employed in Barrett *et al.* (2012).

We take variations $[\frac{\delta}{\delta \vec{Y}^h} \mathcal{L}_2^h](\vec{\eta})$, $[\frac{\delta}{\delta \vec{\kappa}^h} \mathcal{L}_2^h](\vec{\xi})$ and $[\frac{\delta}{\delta \vec{Z}^h} \mathcal{L}_2^h](\chi)$, for $\vec{\xi}, \vec{\eta} \in \underline{V}^h$, $\chi \in W^h$, and set them to zero. This yields (4.18c),

$$\left(G'(|\vec{\kappa}^h|) |\vec{\kappa}^h|^{-1} \vec{\kappa}^h - \vec{Y}^h + Z^h \vec{\tau}^h, \vec{\xi} | \vec{X}_\rho^h | \right)^h = 0 \qquad \forall \, \vec{\xi} \in \underline{V}^h \tag{4.21}$$

and (4.19b).

Taking variations $\vec{\chi} \in \underline{W}^h$ in $\vec{X}^h$, and setting $(\underline{\underline{Q}}^h \vec{X}_t^h, \vec{\chi} | \vec{X}_\rho^h |)^h + \left[\frac{\delta}{\delta \vec{x}} \mathcal{L}_2^h \right](\vec{\chi}) = 0$ we obtain that

$$\left(\underline{\underline{Q}}^h \vec{X}_t^h, \vec{\chi} | \vec{X}_\rho^h | \right)^h + \left(G(|\vec{\kappa}^h|) + \lambda - \vec{\kappa}^h \cdot \vec{Y}^h, \left[\frac{\delta}{\delta \vec{X}^h} | \vec{X}_\rho^h | \right](\vec{\chi}) \right)^h - \left(\vec{Y}_\rho^h, \left[\frac{\delta}{\delta \vec{X}^h} \vec{\tau}^h \right](\vec{\chi}) \right)$$
$$+ \left(Z^h \vec{\kappa}^h, \left[\frac{\delta}{\delta \vec{X}^h} \vec{X}_\rho^h \right](\vec{\chi}) \right)^h = 0 \qquad \forall \, \vec{\chi} \in \underline{W}^h . \tag{4.22}$$

On recalling (4.5), it follows from (4.22) that

$$\left(\underline{\underline{Q}}^h \vec{X}_t^h, \vec{\chi} | \vec{X}_\rho^h | \right)^h + \left(G(|\vec{\kappa}^h|) + \lambda - \vec{\kappa}^h \cdot \vec{Y}^h, \vec{\tau}^h \cdot \vec{\chi}_\rho \right)^h - \left(\vec{Y}_\rho^h, \underline{\underline{P}}^h \vec{\chi}_s \right)$$
$$+ \left(Z^h \vec{\kappa}^h, \vec{\chi}_\rho \right)^h = 0 \qquad \forall \, \vec{\chi} \in \underline{W}^h . \tag{4.23}$$

With (4.14), (4.15) and (4.19b), it follows from choosing $\vec{\xi} = \vec{\theta}^h \in \underline{V}^h$ in (4.21), that

$$\left(\vec{Y}^h - Z^h \vec{\theta}^h, \vec{\theta}^h | \vec{X}_\rho^h | \right)^h = 0 \text{ and } Z^h = \pi_W^h \left[|\vec{\theta}^h|^{-2} \vec{Y}^h \cdot \vec{\theta}^h \right] = \pi_W^h \left[|\vec{\theta}^h|^{-1} \vec{Y}^h \cdot \vec{\omega}_d^h \right]. \tag{4.24}$$

Combining (4.21) and (4.24), yields that

$$\vec{\pi}^h [\underline{\underline{Q}}_\star^h \vec{Y}^h] = \vec{\pi}^h \left[G'(|\vec{\kappa}^h|) |\vec{\kappa}^h|^{-1} \vec{\kappa}^h \right] . \tag{4.25}$$

This gives (4.18b) and inserting Z^h in (4.23) yields (4.18a).

14

Stability. Choosing $\vec{\chi} = \vec{X}_t^h \in \underline{W}^h$ in (4.22), and noting (3.3), yields that

$$\left(|\underline{\underline{Q}}^h\, \vec{X}_t^h|^2, |\vec{X}_\rho^h| \right)^h + \left(G(|\vec{\kappa}^h|) + \lambda - \vec{\kappa}^h \cdot \vec{Y}^h, (|\vec{X}_\rho^h|)_t \right)^h - \left(\vec{Y}_\rho^h, \vec{\tau}_t^h \right)$$
$$+ \left(Z^h\, \vec{\kappa}^h, \vec{X}_{\rho,t}^h \right)^h = 0\,. \tag{4.26}$$

Differentiating (4.18c) with respect to time, and then choosing $\vec{\eta} = \vec{Y}^h$ yields

$$\left(\vec{\kappa}_t^h, \vec{Y}^h\, |\vec{X}_\rho^h| \right)^h + \left(\vec{\kappa}^h \cdot \vec{Y}^h, (|\vec{X}_\rho^h|)_t \right)^h + \left(\vec{Y}_\rho^h, \vec{\tau}_t^h \right) = 0\,, \tag{4.27}$$

i.e. the same as (4.11). Differentiating (4.19b) with respect to t, and then choosing $\chi = Z^h$ yields that

$$\left(Z^h\, \vec{\kappa}_t^h, \vec{X}_\rho^h \right)^h + \left(Z^h\, \vec{\kappa}^h, \vec{X}_{t,\rho}^h \right)^h = 0\,. \tag{4.28}$$

Choosing $\vec{\zeta} = \vec{\kappa}_t^h$ in (4.21) yields that

$$\left(\vec{Y}^h - Z^h\, \vec{\tau}^h, \vec{\kappa}_t^h\, |\vec{X}_\rho^h| \right)^h = \left(G'(|\vec{\kappa}^h|)\, |\vec{\kappa}^h|^{-1}\, \vec{\kappa}^h, \vec{\kappa}_t^h\, |\vec{X}_\rho^h| \right)^h = \left([G(|\vec{\kappa}^h|)]_t, |\vec{X}_\rho^h| \right)^h. \tag{4.29}$$

Combining (4.26), (4.27), (4.28) and (4.29) yields that

$$\begin{aligned}
\frac{\mathrm{d}}{\mathrm{d}t}\, E_\lambda^h(\vec{X}^h, \vec{\kappa}^h) &= \frac{\mathrm{d}}{\mathrm{d}t} \left(G(|\vec{\kappa}^h|), |\vec{X}_\rho^h| \right)^h + \left(\lambda, (|\vec{X}_\rho^h|)_t \right)^h \\
&= \left([G(|\vec{\kappa}^h|)]_t, |\vec{X}_\rho^h| \right)^h + \left(G(|\vec{\kappa}^h|) + \lambda, (|\vec{X}_\rho^h|)_t \right)^h \\
&= \left(\vec{Y}^h - Z^h\, \vec{\tau}^h, \vec{\kappa}_t^h\, |\vec{X}_\rho^h| \right)^h + \left(G(|\vec{\kappa}^h|) + \lambda, (|\vec{X}_\rho^h|)_t \right)^h \\
&= \left(G(|\vec{\kappa}^h|) + \lambda - \vec{\kappa}^h \cdot \vec{Y}^h, (|\vec{X}_\rho^h|)_t \right)^h - \left(\vec{Y}_\rho^h, \vec{\tau}_t^h \right) + \left(Z^h\, \vec{\kappa}^h, \vec{X}_{t,\rho}^h \right)^h \\
&= -\left(|\underline{\underline{Q}}^h\, \vec{X}_t^h|^2, |\vec{X}_\rho^h| \right)^h \le 0\,, \tag{4.30}
\end{aligned}$$

and so a solution satisfying (4.18) is stable.

Equidistribution. Next we show an equidistribution property for the scheme (4.18). Choosing $\vec{\xi} = \vec{\omega}_d^h(q_j)\, \chi_j$ in (4.18b) and $\vec{\eta} = \vec{\omega}_d^h(q_j)\, \chi_j$ in (4.18c), for $j = 1, \ldots, j_1$, yields, on recalling (4.16) and (4.17), that

$$G'(|\vec{\kappa}^h(q_j)|)\, |\vec{\kappa}^h(q_j)|^{-1}\, \vec{\kappa}^h(q_j) \cdot \vec{\omega}_d^h(q_j) = 0\,, \tag{4.31a}$$

$$\vec{\kappa}^h(q_j) \cdot \vec{\omega}_d^h(q_j) \left(\chi_j, |\vec{X}_\rho^h| \right) + \left(\vec{X}_s^h, (\vec{\omega}_d^h(q_j)\, \chi_j)_\rho \right) = 0\,. \tag{4.31b}$$

It follows from (4.31b), on setting $\vec{a}_{j-\frac{1}{2}}^h = \vec{X}(q_j) - \vec{X}(q_{j-1})$ and on noting that $\vec{\omega}_d^h(q_j) = \dfrac{\vec{a}_{j+\frac{1}{2}}^h + \vec{a}_{j-\frac{1}{2}}^h}{|\vec{a}_{j+\frac{1}{2}}^h + \vec{a}_{j-\frac{1}{2}}^h|}$, that

$$\vec{\kappa}^h(q_j) \cdot \vec{\omega}_d^h(q_j) \left(\chi_j, |\vec{X}_\rho^h| \right) + \frac{1}{2} \left(\frac{\vec{a}_{j+\frac{1}{2}}^h}{|\vec{a}_{j+\frac{1}{2}}^h|} - \frac{\vec{a}_{j-\frac{1}{2}}^h}{|\vec{a}_{j-\frac{1}{2}}^h|} \right) \cdot \frac{\vec{a}_{j+\frac{1}{2}}^h + \vec{a}_{j-\frac{1}{2}}^h}{|\vec{a}_{j+\frac{1}{2}}^h + \vec{a}_{j-\frac{1}{2}}^h|} = 0\,. \tag{4.32}$$

If we assume that $G'(z) \neq 0$ for $z > 0$, then it follows from (4.31a) that $|\vec{\kappa}^h(q_j)| = 0$ or that $\vec{\kappa}^h(q_j) \cdot \vec{\omega}_d^h(q_j) = 0$, i.e. the latter always holds. Hence it follows from (4.32) that

$$
\left(\frac{\vec{a}^h_{j+\frac{1}{2}}}{|\vec{a}^h_{j+\frac{1}{2}}|} - \frac{\vec{a}^h_{j-\frac{1}{2}}}{|\vec{a}^h_{j-\frac{1}{2}}|} \right) \cdot \left(\vec{a}^h_{j+\frac{1}{2}} + \vec{a}^h_{j-\frac{1}{2}} \right) = 0 \,, \tag{4.33}
$$

which together with the Cauchy–Schwarz inequality implies that $|\vec{a}^h_{j+\frac{1}{2}}| = |\vec{a}^h_{j-\frac{1}{2}}|$ if $\vec{a}^h_{j+\frac{1}{2}}$ is not parallel to $\vec{a}^h_{j-\frac{1}{2}}$.

Overall we have shown the following results.

THEOREM 2. *Let $G \in C^1(\mathbb{R}_{\geq 0}, \mathbb{R}_{>0})$ satisfy (2.6). Let $(\vec{X}^h(t), \vec{\kappa}^h(t), \vec{Y}^h(t))_{t\in(0,T]}$ denote a solution to (4.18), with $(\vec{X}^h(t))_{t\in(0,T]}$ satisfying $(\mathcal{C}_2^h)$. Then it holds that*

$$
\frac{\mathrm{d}}{\mathrm{d}t} E_\lambda^h(\vec{X}^h, \vec{\kappa}^h) + \left(|\underline{\underline{Q}}^h \, \vec{X}_t^h|^2, |\vec{X}_\rho^h| \right)^h = 0 \,.
$$

Moreover, if $G'(z) \neq 0$ for $z > 0$, then on letting $\vec{a}^h_{j+\frac{1}{2}} = \vec{X}^h(q_j, t) - \vec{X}^h(q_{j+1}, t)$, $j = 0, \ldots, j_1$, for a fixed time $t \in (0, T]$, it holds for $j = 1, \ldots, j_1$ that

$$
|\vec{a}^h_{j+\frac{1}{2}}| = |\vec{a}^h_{j-\frac{1}{2}}| \quad \text{if} \quad \vec{a}^h_{j+\frac{1}{2}} \nparallel \vec{a}^h_{j-\frac{1}{2}} \,.
$$

REMARK 3. *We note that the assumption $G'(z) \neq 0$ for $z > 0$ is satisfied for all the choices in (1.3). The proof of the equidistribution properties highlights that a weaker sufficient condition is given by $G'(|\vec{\kappa}^h(q_j)|) \neq 0$, for $j = 1, \ldots, j_1$.*

We also stress that the equidistribution property is what sets the approximation (4.18) apart from (4.7), and this is what makes fully discrete variants of the former more practical than fully discrete versions of the latter.

5 Fully discrete finite element approximation

5.1 Fully discrete scheme without tangential motion

On recalling (4.7) we introduce the following fully discrete approximation of (3.4). Given $\vec{X}^0 \in \underline{V}^h$ with $\vec{X}^0(q) = \vec{\alpha}_q$ for $q \in \partial I$ and suitably chosen $\vec{\kappa}^0 \in \underline{V}^h$ and $\vec{Y}^0 \in \underline{V}^h$, find $(\delta\vec{X}^{m+1}, \vec{\kappa}^{m+1}, \vec{Y}^{m+1}) \in \underline{W}^h \times \underline{V}^h \times \underline{V}^h$, with $\vec{X}^{m+1} = \vec{X}^m + \delta\vec{X}^{m+1}$, such that for

$m = 0, \ldots, M-1$

$$\frac{1}{\Delta t_m} \left(\delta \vec{X}^{m+1}, \vec{\chi} \, | \vec{X}_\rho^m | \right)^h - \left(\underline{\underline{P}}^m \, \vec{Y}_s^{m+1}, \vec{\chi}_s \, | \vec{X}_\rho^m | \right)$$

$$= - \left([G(|\vec{\kappa}^m|) + \lambda - \vec{\kappa}^m \cdot \vec{Y}^m] \, \vec{X}_s^m, \vec{\chi}_s \, | \vec{X}_\rho^m | \right)^h \qquad \forall \, \vec{\chi} \in \underline{W}^h, \quad (5.1a)$$

$$\left(G'(|\vec{\kappa}^{m+1}|) \, |\vec{\kappa}^{m+1}|^{-1} \, \vec{\kappa}^{m+1} - \vec{Y}^{m+1}, \vec{\xi} \, | \vec{X}_\rho^m | \right)^h = 0 \qquad \forall \, \vec{\xi} \in \underline{V}^h, \quad (5.1b)$$

$$\left(\vec{\kappa}^{m+1}, \vec{\eta} \, | \vec{X}_\rho^m | \right)^h + \left(\vec{X}_s^{m+1}, \vec{\eta}_s \, | \vec{X}_\rho^m | \right) = \sum_{q \in \partial I} \vec{\zeta}_q \cdot \vec{\eta}(q) \quad \forall \, \vec{\eta} \in \underline{V}^h. \quad (5.1c)$$

We observe that in the case (1.3a) with $p = 2$, it follows from (5.1b) that $\vec{\kappa}^{m+1} = \vec{Y}^{m+1}$, and so the scheme (5.1), in the case $I = \mathbb{R}/\mathbb{Z}$, collapses to a fully discrete variant of the scheme (2.9), (2.10) in Deckelnick and Dziuk (2009) for elastic flow, compare also with Barrett *et al.* (2010, (3.7)).

5.2   Fully discrete scheme with tangential motion

Built on (4.18) we introduce the following fully discrete approximation of (3.10). Given $\vec{X}^0 \in \underline{V}^h$ with $\vec{X}^0(q) = \vec{\alpha}_q$ for $q \in \partial I$ and suitably chosen $\vec{\kappa}^0 \in \underline{V}^h$ and $\vec{Y}^0 \in \underline{V}^h$, find $(\delta \vec{X}^{m+1}, \vec{\kappa}^{m+1}, \vec{Y}^{m+1}) \in \underline{W}^h \times \underline{V}^h \times \underline{V}^h$, with $\vec{X}^{m+1} = \vec{X}^m + \delta \vec{X}^{m+1}$, such that for $m = 0, \ldots, M-1$

$$\frac{1}{\Delta t_m} \left(\underline{\underline{Q}}_\star^m \, \delta \vec{X}^{m+1}, \vec{\chi} \, | \vec{X}_\rho^m | \right)^h - \left(\vec{Y}_s^{m+1}, \vec{\chi}_s \, | \vec{X}_\rho^m | \right) + \left((\vec{\mathrm{Id}} - \underline{\underline{P}}^m) \, \vec{Y}_s^m, \vec{\chi}_s \, | \vec{X}_\rho^m | \right)$$

$$= - \left([G(|\vec{\kappa}^m|) + \lambda - \vec{\kappa}^m \cdot \vec{Y}^m] \, \vec{X}_s^m, \vec{\chi}_s \, | \vec{X}_\rho^m | \right)^h$$

$$- \left(\pi_W^h \, [|\vec{\theta}^m|^{-1} \, (\vec{Y}^m \cdot \vec{\omega}_d^m)] \, \vec{\kappa}^m, \vec{\chi}_s \, | \vec{X}_\rho^m | \right)^h \qquad \forall \, \vec{\chi} \in \underline{W}^h, \quad (5.2a)$$

$$\left(G'(|\vec{\kappa}^{m+1}|) \, |\vec{\kappa}^{m+1}|^{-1} \, \vec{\kappa}^{m+1} - \underline{\underline{Q}}_\star^m \, \vec{Y}^{m+1}, \vec{\xi} \, | \vec{X}_\rho^m | \right)^h = 0 \qquad \forall \, \vec{\xi} \in \underline{V}^h, \quad (5.2b)$$

$$\left(\vec{\kappa}^{m+1}, \vec{\eta} \, | \vec{X}_\rho^m | \right)^h + \left(\vec{X}_s^{m+1}, \vec{\eta}_s \, | \vec{X}_\rho^m | \right) = \sum_{q \in \partial I} \vec{\zeta}_q \cdot \vec{\eta}(q) \quad \forall \, \vec{\eta} \in \underline{V}^h. \quad (5.2c)$$

Here we have introduced the time discrete analogue $\underline{\underline{Q}}_\star^m$ of (4.17). As $\delta \vec{X}^{m+1} \in \underline{W}^h$ it follows that $\underline{\underline{Q}}_\star^m$ in the first term in (5.2a) can be replaced by $\underline{\underline{Q}}^m$.

REMARK 4.

- *We observe that in the case (1.3a) with $p = 2$, it follows from (5.2b) that $\vec{\kappa}^{m+1} = \vec{\pi}^h \, [\underline{\underline{Q}}_\star^m \, \vec{Y}^{m+1}]$, and so our scheme (5.2) collapses to the linear schemes (4.1), if $I = \mathbb{R}/\mathbb{Z}$, and (4.9), if $I = (0, 1)$, in Barrett* et al. *(2012). We recall from Barrett* et al. *(2012, Theorems 4.1 and 4.3) that these schemes admit a unique solution, and this is the reason for the chosen time-discretisation of the terms involving $\vec{Y}^{m+1}$ and $\vec{Y}^m$ in (5.2a); see also Barrett* et al. *(2012, Remark 4.1).*

17

- *For general G, the scheme (5.2) is (mildly) nonlinear, and can be solved with the help of a Newton iterative solver. An alternative, linear scheme can be obtained by replacing $G'(|\vec{\kappa}^{m+1}|)\,|\vec{\kappa}^{m+1}|^{-1}$ in (5.2b) with $G'(|\vec{\kappa}^m|)\,|\vec{\kappa}^m|^{-1}$. However, in practice such a scheme does not perform well, with the scheme breaking down, for example because $|\vec{\kappa}^{m+1}|$ becomes too small. That is why we prefer the nonlinear scheme (5.2).*
- *The main difference between the two schemes (5.1) and (5.2) is that the former uses the standard discrete curvature vector $\vec{\kappa}^{m+1}$ as a variable, which leads to mainly normal motion for $\vec{X}^{m+1}$. This is in the spirit of the seminal works by Dziuk, see e.g. Dziuk (1991, 1994, 2008); Deckelnick and Dziuk (2009). The scheme (5.2), on the other hand, enforces $\vec{\kappa}^{m+1}$ to have no tangential components, which leads to an implicit tangential motion in $\vec{X}^{m+1}$ that gives equidistributed meshes, at least in the semidiscrete limit, recall Theorem 2. This is in the spirit of the works by Barrett, Garcke and Nürnberg, see e.g. Barrett et al. (2010, 2011, 2012) for the case of discrete curve evolutions.*

5.3 Solution of the nonlinear system of equations

With the obvious abuse of notation, i.e. on letting $\vec{Y}^{m+1}$, $\delta\vec{X}^{m+1}$, κ^{m+1} also denote the vector of coefficients with respect to the basis functions of $\underline{V}^h$, we can write the nonlinear systems (5.1) and (5.2) as

$$
\begin{pmatrix}
\underline{\underline{A}} & -\frac{1}{\Delta t_m}\underline{\underline{\mathcal{M}}} & 0 \\
0 & \underline{\underline{A}} & \underline{M} \\
-\underline{\underline{\mathcal{M}}} & 0 & \underline{\underline{M}}_G(\vec{\kappa}^{m+1})
\end{pmatrix}
\begin{pmatrix}
\vec{Y}^{m+1} \\
\delta\vec{X}^{m+1} \\
\vec{\kappa}^{m+1}
\end{pmatrix}
=
\begin{pmatrix}
\vec{g}^m \\
\vec{f}^m \\
\vec{0}
\end{pmatrix},
\tag{5.3}
$$

where the definitions of the matrices and vectors in (5.3) follow from (5.1) and (5.2). In particular, for (5.2), and in the case $I = \mathbb{R}/\mathbb{Z}$, the block diagonal matrices $\underline{\underline{\mathcal{M}}}$, $\underline{\underline{M}}_G(\vec{\kappa}^{m+1})$ and $\underline{M}$ are defined by their diagonal block entries

$$
\underline{\underline{\mathcal{M}}}_{jj} = M_{jj}\,\underline{Q}_\star^m(q_j)\,, \quad [\underline{\underline{M}}_G(\vec{\kappa}^{m+1})]_{jj} = G'(|\vec{\kappa}^{m+1}(q_j)|)\,|\vec{\kappa}^{m+1}(q_j)|^{-1}\,M_{jj}\,\underline{\mathrm{Id}}\,,
$$

$$
\underline{\underline{M}}_{jj} = M_{jj}\,\underline{\mathrm{Id}}\,, \quad M_{jj} = \left(\chi_j, |\vec{X}_\rho^m|\right), j = j_0, \dots, J\,.
\tag{5.4}
$$

The Jacobian matrix of (5.3) at a Newton iterate $(\vec{Y}^N, \delta\vec{X}^N, \vec{\kappa}^N)^T$ is independent of $\vec{Y}^N, \delta\vec{X}^N$, and can be written as

$$
\begin{pmatrix}
\underline{\underline{A}} & -\frac{1}{\Delta t_m}\underline{\underline{\mathcal{M}}} & 0 \\
0 & \underline{\underline{A}} & \underline{M} \\
-\underline{\underline{\mathcal{M}}} & 0 & \underline{\underline{M}}_{dG}(\vec{\kappa}^N)
\end{pmatrix},
\tag{5.5}
$$

where

$$
[\underline{\underline{M}}_{dG}(\vec{\kappa}^N)]_{jj} = M_{jj}\,\big(G'(|\vec{\kappa}^N(q_j)|)\,|\vec{\kappa}^N(q_j)|^{-1}\,\underline{\mathrm{Id}}
$$
$$
+\,[G''(|\vec{\kappa}^N(q_j)|) - G'(|\vec{\kappa}^N(q_j)|)\,|\vec{\kappa}^N(q_j)|^{-1}]\,|\vec{\kappa}^N(q_j)|^{-2}\,\vec{\kappa}^N(q_j)\otimes\vec{\kappa}^N(q_j)\big)\,.
\tag{5.6}
$$

18

We note that for the cases (1.3a)–(1.3c) we have

$$G'(z)/z = z^{p-2}\,, \qquad\qquad G''(z) = (p-1)\,z^{p-2}\,, \qquad\qquad (5.7a)$$

$$G'(z)/z = \alpha\,z^{-3}\,e^{-\alpha/z}\,, \qquad\qquad G''(z) = \alpha\,(\alpha - 2\,z)\,z^{-4}\,e^{-\alpha/z}\,, \qquad\qquad (5.7b)$$

$$G'(z)/z = \tfrac{1}{2}\,z^{-\frac{5}{2}}\,(z + 2\,\alpha)\,e^{-\alpha/z}\,, \quad G''(z) = \tfrac{1}{4}\,z^{-\frac{7}{2}}\,(z^2 + 4\,\alpha\,z - 4\,\alpha^2)\,e^{-\alpha/z}\,. \qquad (5.7c)$$

In practice the Newton iteration for (5.3), for the schemes (5.1) and (5.2), usually converges in only a few steps. We implemented the schemes (5.1) and (5.2) with the help of the finite element toolbox ALBERTA, see Schmidt and Siebert (2005). The linear subproblems of the Newton iteration, featuring the block matrix (5.5), are solved with the help of the sparse factorization package UMFPACK, see Davis (2004).

6   Numerical results

Throughout the numerical experiments we take, for given $\vec{X}_0$, $\vec{\kappa}^0 = \underline{\underline{Q}}^0\,\vec{k}$, where $\vec{k} \in \underline{V}^h$ is the solution to

$$\left(\vec{k}, \vec{\eta}\,|\vec{X}_\rho^0|\right)^h + \left(\vec{X}_s^0, \vec{\eta}_s\,|\vec{X}_\rho^0|\right) = \sum_{q \in \partial I} \vec{\zeta}_q \cdot \vec{\eta}(q) \qquad \forall\,\vec{\eta} \in \underline{V}^h\,,$$

and then set $\vec{Y}^0 = \vec{\pi}^h\,[G'(|\vec{\kappa}^0|)\,|\vec{\kappa}^0|^{-1}\,\vec{\kappa}^0]$. We will always employ uniform time steps, $\Delta t_m = \Delta t$, $m = 0,\ldots,M-1$. For the spatial resolution we will refer to h_{Γ^0}, the maximal edge length of Γ^0. On recalling (4.6), we will refer to $E_\lambda^h(\vec{X}^m, \vec{\kappa}^{m+1})$ as the fully discrete energy for solutions of the schemes (5.1) and (5.2), respectively. We stress that no remeshing was used in any of the experiments presented in this section.

6.1   Numerical results for $d = 2$

6.1.1   Circular solutions

For the choice (1.3a), we recall the true solution (A.6) with (A.11) for (2.13) with $\lambda = 0$ from the appendix. It will be used for the convergence tests for the presented schemes. To this end, we start with the initial data

$$\vec{X}^0(q_j) = r(0)\begin{pmatrix}\cos[2\,\pi\,q_j + 0.1\,\sin(2\,\pi\,q_j)]\\ \sin[2\,\pi\,q_j + 0.1\,\sin(2\,\pi\,q_j)]\end{pmatrix}, \quad j = 1,\ldots,J\,, \qquad (6.1)$$

recall (4.1), with $r(0) = 1$. We compute the error

$$\|\Gamma - \Gamma^h\|_{L^\infty} = \max_{m=1,\ldots,M}\ \max_{j=1,\ldots,J}\ \bigl||\vec{X}^m(q_j)| - r(t_m)\bigr| \qquad (6.2)$$

over the time interval $[0, 1]$ between the true solution and the discrete solutions. Here we use the time step size $\Delta t = 0.1\,h_{\Gamma^0}^2$. For the choices $p = 2$, $p = 5$ and $p = 1.1$ the

		(5.1)		(5.2)	
J	h_{Γ^0}	$\|\Gamma - \Gamma^h\|_{L^\infty}$	EOC	$\|\Gamma - \Gamma^h\|_{L^\infty}$	EOC
32	2.1544e-01	2.1279e-03	—	2.2720e-03	—
64	1.0792e-01	5.3401e-04	2.00	5.6804e-04	2.01
128	5.3988e-02	1.3363e-04	2.00	1.4201e-04	2.00
256	2.6997e-02	3.3416e-05	2.00	3.5503e-05	2.00
512	1.3499e-02	8.3546e-06	2.00	8.8759e-06	2.00

Table 1: Convergence test for (1.3a), $p = 2$, $\lambda = 0$, over the time interval $[0, 1]$.

		(5.1)		(5.2)	
J	h_{Γ^0}	$\|\Gamma - \Gamma^h\|_{L^\infty}$	EOC	$\|\Gamma - \Gamma^h\|_{L^\infty}$	EOC
32	2.1544e-01	3.2297e-03	—	4.2993e-03	—
64	1.0792e-01	8.0173e-04	2.02	1.0631e-03	2.02
128	5.3988e-02	2.0008e-04	2.00	2.6507e-04	2.01
256	2.6997e-02	5.0001e-05	2.00	6.6227e-05	2.00
512	1.3499e-02	1.2499e-05	2.00	1.6554e-05	2.00

Table 2: Convergence test for (1.3a), $p = 5$, $\lambda = 0$, over the time interval $[0, 1]$.

		(5.1)		(5.2)	
J	h_{Γ^0}	$\|\Gamma - \Gamma^h\|_{L^\infty}$	EOC	$\|\Gamma - \Gamma^h\|_{L^\infty}$	EOC
32	2.1544e-01	8.9127e-04	—	1.4774e-04	—
64	1.0792e-01	2.2636e-04	1.98	3.7037e-05	2.00
128	5.3988e-02	5.6815e-05	2.00	9.2660e-06	2.00
256	2.6997e-02	1.4218e-05	2.00	2.3169e-06	2.00
512	1.3499e-02	3.5554e-06	2.00	5.7926e-07	2.00

Table 3: Convergence test for (1.3a), $p = 1.1$, $\lambda = 0$, over the time interval $[0, 1]$.

J	h_{Γ^0}	(5.1) $\|\Gamma - \Gamma^h\|_{L^\infty}$	EOC	(5.2) $\|\Gamma - \Gamma^h\|_{L^\infty}$	EOC
32	2.1544e-01	4.5099e-04	—	2.1356e-04	—
64	1.0792e-01	1.1368e-04	1.99	5.3519e-05	2.00
128	5.3988e-02	2.8479e-05	2.00	1.3156e-05	2.03
256	2.6997e-02	7.1234e-06	2.00	2.2891e-06	2.52
512	1.3499e-02	1.7811e-06	2.00	5.7227e-07	2.00

Table 4: Convergence test for (1.3b), $\alpha = 4$, $\lambda = 0$, over the time interval $[0, 1]$.
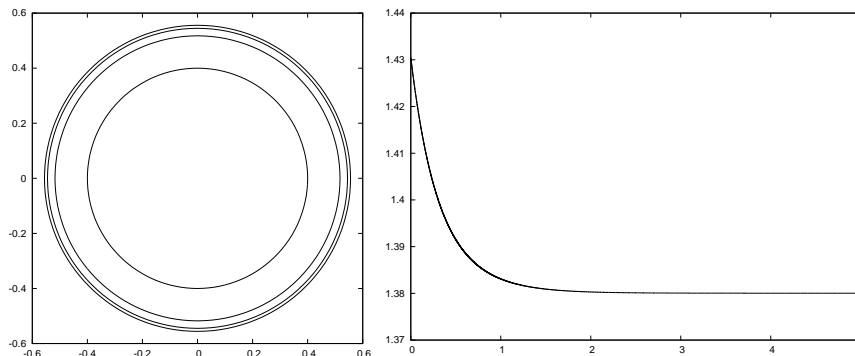
Figure 1: (1.3c) with $\alpha = 4$, $\lambda = 0.25$. Left: Plots of the curve at times $t = 0, 1, 2, 5$. Right: t vs discrete energy on $[0, 5]$.

computed errors are reported in Tables 1–3. In each case we observe that the schemes exhibit second order convergence rates.

For the choice (1.3b), we use a numerical solution of the differential equation (A.6) with (A.13), from the appendix, for (2.13) with $\lambda = 0$. For the presented convergence tests, we start with the initial data (6.1) with $r(0) = 0.5$. We compute the error (6.2) over the time interval $[0, 1]$. Here we use the time step size $\Delta t = 0.1 \, h_{\Gamma^0}^2$. For the choice $\alpha = 4$ the computed errors are reported in Table 4.

For (1.3c), we now investigate the behaviour of circles close to stationary radial solutions with radius r such that $r^{-\frac{1}{2}} e^{-\alpha r} \left(\frac{1}{2} - \alpha r \right) + \lambda = 0$, recall (A.19) in the appendix. To this end, we numerically compute the stationary radius $r \approx 0.55617$ for $\alpha = 4$ and $\lambda = 0.25$, see Figure 11 (right). On noting (A.19) we observe that this stationary solution is stable. Indeed, starting with the initial data (6.1) with $r(0) = 0.4$ and $J = 128$, we use the scheme (5.2) to compute the evolution shown in Figure 1. Here we use the very small time step size $\Delta t = 10^{-7}$, since for larger values the Newton iteration to solve the nonlinear equations arising at each time step does not converge. With the chosen Δt, the maximum number of Newton iterations per time step was 2. We note that at the final time the discrete curve has a diameter of 1.112, which is approximately twice the expected radius of the stationary solution.

		(5.1)		(5.2)	
J	h_{Γ^0}	$\|\Gamma(1) - \Gamma^M\|$	EOC	$\|\Gamma(1) - \Gamma^M\|$	EOC
32	1.0792e-01	3.0545e-05	—	2.7926e-05	—
64	5.3988e-02	4.1892e-06	2.87	3.6824e-06	2.93
128	2.6997e-02	6.1270e-07	2.77	5.0761e-07	2.86
256	1.3499e-02	9.9239e-08	2.63	7.5317e-08	2.75
512	6.7495e-03	1.8154e-08	2.45	1.2393e-08	2.60

Table 5: Convergence test for clamped boundary conditions for (1.3a), $p = 4$, with $\lambda = \frac{3}{4}$ and $\vec{\zeta}_0 = \vec{\zeta}_1 = -\vec{e}_2$.
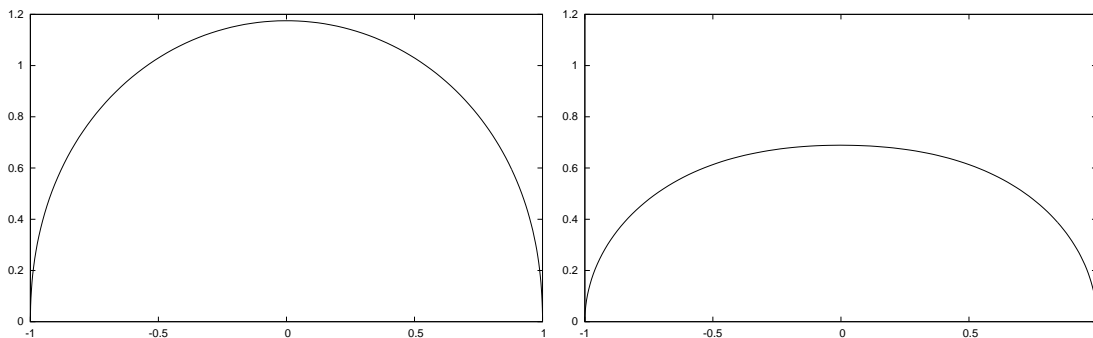
Figure 2: Steady state solutions for (1.3a) with $p = 4$ and clamped boundary conditions $\vec{\zeta}_0 = \vec{\zeta}_1 = -\vec{e}_2$. Left: $\lambda = 0.01$. Right: $\lambda = 10$.

6.1.2 Clamped boundary conditions

In order to test the convergence of the schemes in the presence of clamped boundary conditions, we consider the stable stationary solution for (1.3a) with $r = 1$ and $\lambda = \frac{p-1}{p}$, recall (A.19) in the appendix. Similarly to (6.1), we choose the initial data

$$\vec{X}^0(q_j) = \begin{pmatrix} \sin[(q_j - \frac{1}{2})\,\pi + 0.1\,\cos((q_j - \frac{1}{2})\,\pi)] \\ \cos[(q_j - \frac{1}{2})\,\pi + 0.1\,\cos((q_j - \frac{1}{2})\,\pi)] \end{pmatrix}, \quad j = 0, \ldots, J, \qquad (6.3)$$

and provide the boundary conditions defined by X^0 and $\vec{\zeta}_0 = \vec{\zeta}_1 = -\vec{e}_2$. On computing the solution until time $t = 1$, with $\Delta t = 0.1\,h_{\Gamma^0}^2$, we compute the maximal distance between $\vec{X}^M(q_j)$ and the unit semicircle. For the choice $p = 4$, the results are presented in Table 5. As we start the simulations with an interpolation of the true steady state solution, we observe some superconvergence for large h_{Γ^0}. But eventually the convergence rates seem to settle on second order.

For the same setup as for Table 5, we now present a simulation each with $\lambda < \frac{3}{4}$ and $\lambda > \frac{3}{4}$, so that the unit semicircle is no longer a stationary solution. The plots of the obtained numerical steady state solutions, for the scheme (5.2) with $J = 128$ and $\Delta t = 10^{-3}$, are shown in Figure 2.
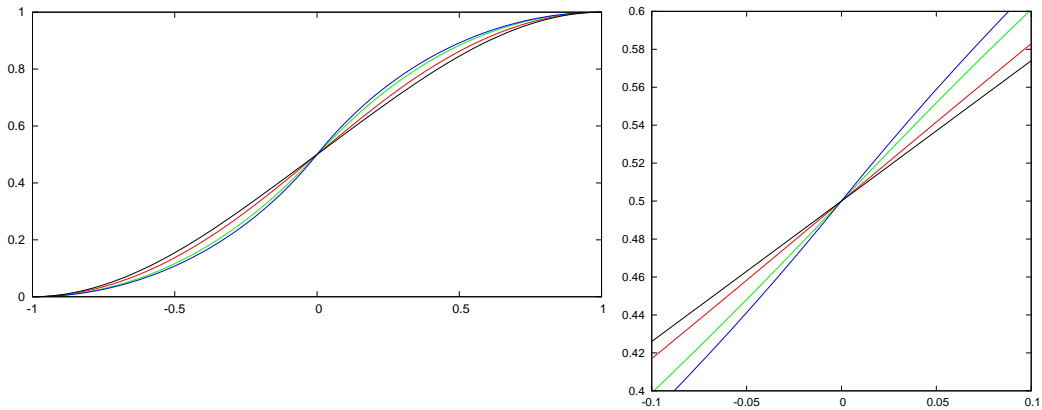
22

Figure 3: Steady state solutions for (1.3a) with $p = 1.6$ (black), $p = 2$ (red), $p = 4$ (green) and $p = 15$ (blue), $\lambda = 0.1$ and clamped boundary conditions $\vec{\zeta}_1 = -\vec{\zeta}_0 = \vec{e}_1$. A closeup around the point $(0, 0.5)^T$ on the right.

In the next experiment, we connect two horizontal lines by a minimising curve. In Figure 3, we show the comparison of the obtained discrete approximations to the minimisers for the energy (2.5), with $\lambda = 0.1$, for (1.3a) with $p \in \{1.6, 2, 4, 15\}$. Here we use the scheme (5.2) with $J = 128$ and $\tau = 10^{-5}$. We note that for $p < 2$ the steady state solution becomes more straight, while for $p > 2$ the shape is more curved. In other words, for $p < 2$ the maximal curvature and the length of the curve become smaller, while for $p > 2$ both become larger. The discrete energies for the displayed solutions are 0.963, 0.791, 0.421 and 0.236, respectively.

In order to allow simulations of the situation in Figure 3 for the choice (1.3b), we apply a regularisation term and consider

$$G(z) = e^{-\alpha/z} + \tfrac{1}{2}\,\varepsilon\,z^2 \quad \text{with } \varepsilon = 10^{-12}\,. \tag{6.4}$$

This is purely to help overcome numerical difficulties when $|z|$ is small, and, as far as we can establish, this has no major influence on the computed evolution. For example, the errors in Table 4 for the scheme (5.2), but with (1.3b) replaced by (6.4), are given by 2.1361e-04, 5.3522e-05, 1.3388e-05, 3.3475e-06, 8.3687e-07. In Figure 4, we show the comparison of the obtained discrete approximations to the minimisers for the energy (2.5), with $\lambda = 0.1$, for (6.4) with $\alpha \in \{3, 4, 9, 15\}$. Here we use the scheme (5.2) with $J = 128$ and $\tau = 10^{-5}$. We observe that, in contrast to Figure 3, the arrangements of the stationary curves is not monotone in the parameter α. In particular, the curve for $\alpha = 3$ lies between the curves for $\alpha = 4$ and $\alpha = 9$. In fact, further numerical investigations suggest that $\alpha = 4$ is approximately the value that leads to the largest deformation of the stationary curve. The discrete energies for the solutions displayed in Figure 4 are 0.271, 0.243, 0.228 and 0.226, respectively.
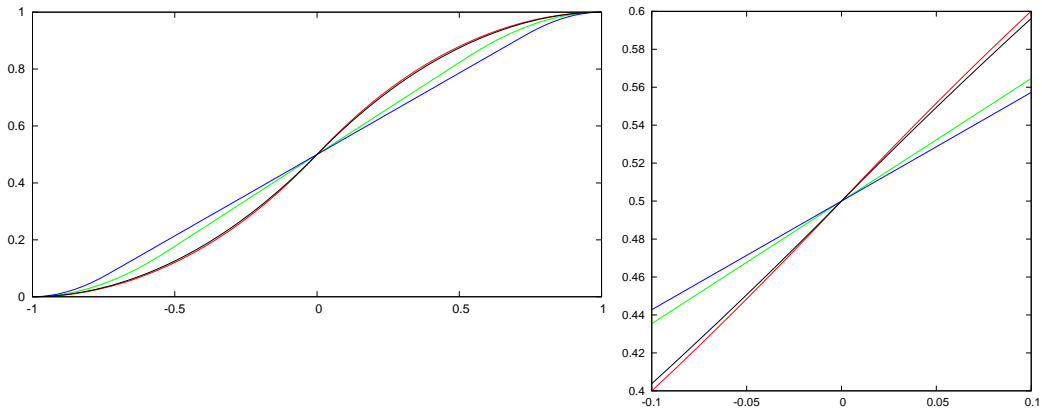
23

Figure 4: Left: Steady state solutions for (6.4) with $\alpha = 3$ (black), $\alpha = 4$ (red), $\alpha = 9$ (green) and $\alpha = 15$ (blue), $\lambda = 0.1$ and clamped boundary conditions $\vec{\zeta_1} = -\vec{\zeta_0} = \vec{e}_1$. Right: A closeup around the point $(0, 0.5)^T$.

6.2 Numerical results for $d = 3$

Here we only consider clamped boundary conditions, since we expect stationary closed curves to lie within two-dimensional hyperplanes. Throughout this subsection, we let $\lambda = 1$ and choose the discretisation parameters $J = 512$ and $\Delta t = 10^{-4}$. Unless otherwise stated, we employ the scheme (5.2).

We begin with an evolution for a segment of a helix, parameterised by

$$\vec{x}_0(\rho) = \left[\rho, \sin(2\pi\rho), \cos(2\pi\rho)\right]^T \qquad \forall\, \rho \in [0, 1],$$

for the clamped boundary conditions (2.3) given by $\vec{x}_0$ and $\vec{\zeta_1} = -\vec{\zeta_0} = \vec{e}_2$. For the energy induced by (1.3a) with $p = 1.5$, the initially three-dimensional curve collapses to a curve that lies in a hyperplane parallel to the $x - y$–plane. See Figure 5 for the evolution. The energy plot nicely illustrates the rapid decay of the energy as the curve settles into the two-dimensional hyperplane, where it appears to have reached a steady state. The discrete energy for the final solution in Figure 5 is 7.71.

For (1.3a) with $p \in \{2, 4, 15\}$, however, the curve remains three-dimensional throughout, until it settles on a stationary shape, see Figure 6. Similarly to Figure 3, we observe that larger values of p lead to curves with higher maximal curvature and greater overall length. The discrete energies for the solutions displayed in Figure 6 are 8.67, 7.70 and 6.65, respectively. We remark that starting the evolution from the final shape in Figure 5, for $p = \{2, 4, 15\}$, still leads to the stationary solutions displayed in Figure 6. Hence we conjecture that these solutions are indeed discrete approximations to the global minimiser for the considered curvature energy and the prescribed clamped boundary conditions.

Moreover, we conjecture that the global minimiser changes from a planar to a non-planar shape for a critical value of p. As an explanation we can state that the curvature-term gets more expensive for larger p and starts to dominate the term that penalises the length of the curve. To study this further, we computed for a set of p-values in
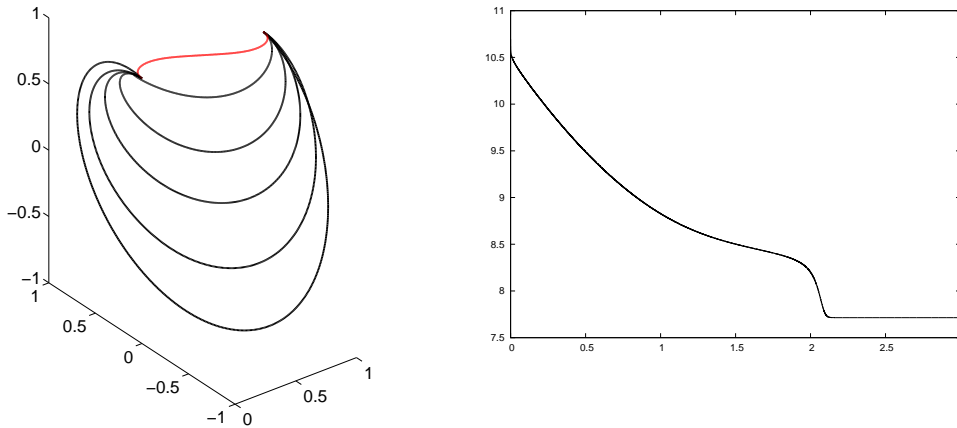
24

Figure 5: Evolution of a helical curve. (1.3a) with $p = 1.5$, $\lambda = 1$, $\vec{\zeta_1} = -\vec{\zeta_0} = \vec{e}_2$. Left: Plots of the curve at times $t = 0, 0.5, \ldots, 2.5$, with the almost stationary (planar) curve at time $t = 2.5$ in red. Right: t vs discrete energy on $[0.3]$.
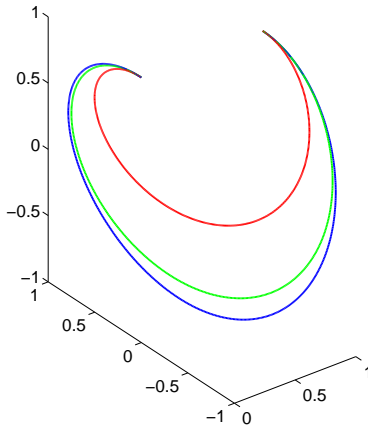

Figure 6: Non-planar steady state solutions for (1.3a) with $\lambda = 1$, $\vec{\zeta_1} = -\vec{\zeta_0} = \vec{e}_2$ and $p = 2$ (red), $p = 4$ (green) and $p = 15$ (blue).

$[1.5, 2]$, and for two possible initial curves (either planar (2d), or non-planar (3d)), the diameter in z-direction of the stationary solution, see Figure 7. It can be seen that for values $p \in [1.55, 1.81]$, two different stationary states appear to exist (planar and non-planar), and the initial data critically determines which state is reached. Moreover, by comparing the energy of the final states, we conjecture that the planar stationary state is the minimiser for $p < 1.63$, while the non-planar curve is the minimiser for $p > 1.64$.

We remark that the scheme (5.1) is not able to integrate the evolution in Figure 5 with the same discretisation parameters. Even if we choose the much smaller time step size $\Delta t = 10^{-6}$, the scheme (5.1) can only compute the evolution until about $t = 1.4$, at which point the scheme breaks down due to coalescence of mesh points. In Figure 8 we compare the element ratio

$$\mathfrak{r}^m = \frac{\max_{j=1 \to J} |\vec{X}^m(q_j) - \vec{X}^m(q_{j-1})|}{\min_{j=1 \to J} |\vec{X}^m(q_j) - \vec{X}^m(q_{j-1})|} \tag{6.5}$$
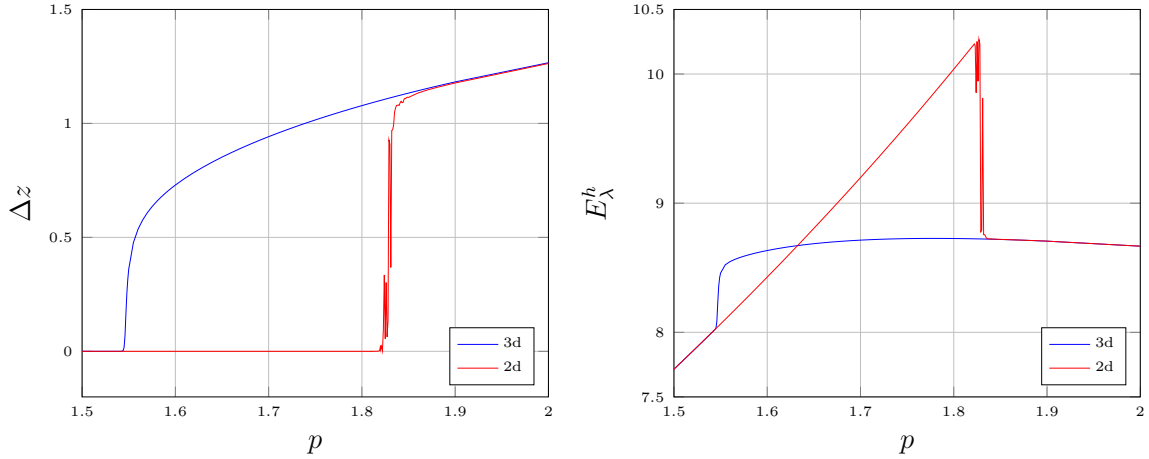
25

Figure 7: A plot of $\Delta z = \max_{j,\ell=0,\dots,J} |(\vec{X}^M(q_j) - \vec{X}^M(q_\ell)) \cdot \vec{e}_2|$ (left) and the discrete energy E_λ^h (right) against p in (1.3a). Here we show a curve each for two-dimensional (red) and three-dimensional (blue) initial data, respectively.
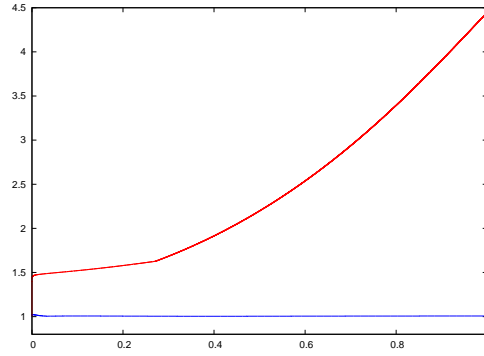

Figure 8: The time evolution of the ratio (6.5) for the schemes (5.1) (red) and (5.2) (blue) for the experiment as in Figure 5 with $\Delta t = 10^{-6}$.

for the schemes (5.1) and (5.2) for this simulation with $\Delta t = 10^{-6}$ until time $t = 1$. It can be clearly seen that for the scheme (5.1) the ratio increases dramatically, while for the scheme (5.2) the ratio converges to 1, meaning an equidistribution of the vertices.

Finally, for (1.3a) with $p \in \{1.5, 4\}$, we show some more involved evolutions towards the steady states shown in Figures 5 and 6. To this end, we choose as initial data a discretisation of

$$\vec{x}_0(\rho) = \big[\rho, \sin(4\,\pi\rho), \cos(4\,\pi\,\rho)\big]^T \qquad \forall\, \rho \in [0,1],$$

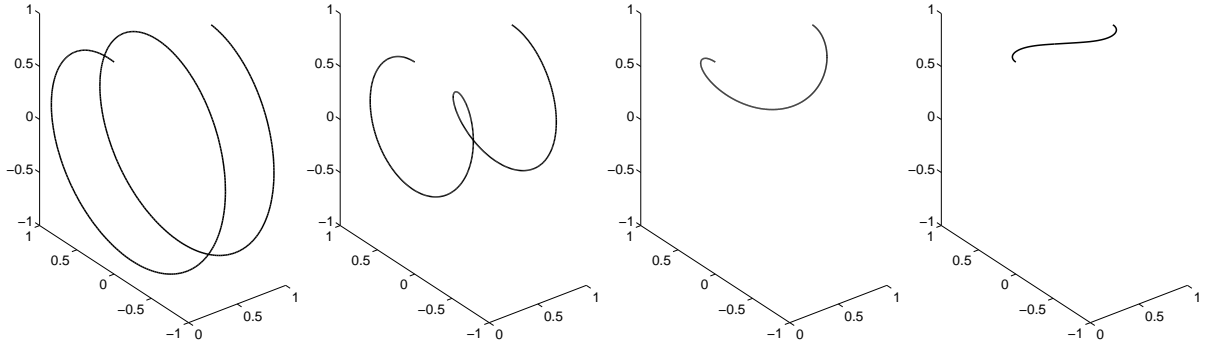i.e. a helix with two turns. The computed evolutions are shown in Figures 9 and 10.

Figure 9: Evolution of a double-winded helical curve. (1.3a) with $p = 1.5$, $\lambda = 1$, $\vec{\zeta}_1 = -\vec{\zeta}_0 = \vec{e}_2$. The convergence is towards the steady state solution shown in Figure 5. The curve is shown at times $t = 0, 1, 2, 5$ (from left to right).
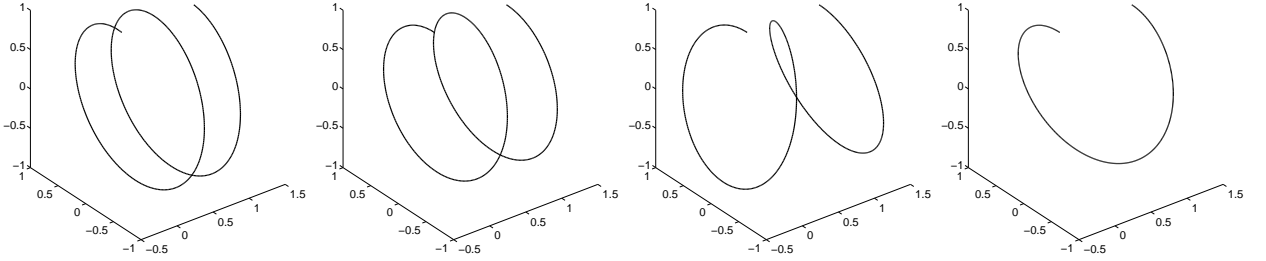

Figure 10: (1.3a) with $p = 4$, $\lambda = 1$, $\vec{\zeta}_1 = -\vec{\zeta}_0 = \vec{e}_2$. Evolution of a clamped helix towards the steady state solution shown in Figure 6. The curve is shown at times $t = 0, 5, 10, 20$.

Conclusion

We have presented two continuous-in-time semidiscrete finite element discretisations for the approximation of the L^2–gradient flow of general curvature energies of the form (2.5), featuring a general energy density G. Here we have considered closed and open curves, taking into account clamped boundary conditions in the case of open curves. Both schemes can be shown to be stable, and the second variant satisfies, in addition, an equidistribution property. The introduced corresponding fully discrete approximations, (5.1) and (5.2), are in general mildly nonlinear, due to the possible nonlinearities present in G'. In practice both schemes perform well in convergence tests, using exact radial solutions developed in the appendix, and exhibit good stability properties. The scheme (5.2) proved to be more robust in practice, as (5.1) could at times not compute evolutions unless the time discretisation parameter was chosen sufficiently small. Moreover, the scheme (5.1) can suffer from coalescence in practice, while the vertices for scheme (5.2) are always well distributed.

A   Exact radial solutions for $d = 2$

General planar curves   For a closed curve in the case $d = 2$ we can define the normal to the curve via

$$\vec{\nu} = -\vec{\tau}^{\perp} \,, \tag{A.1}$$

where $(\cdot)^{\perp}$ denotes a clockwise rotation by $\frac{\pi}{2}$. Then we can introduce the curve's scalar curvature via

$$\varkappa \vec{\nu} = \vec{\varkappa} = \vec{\tau}_s = \vec{x}_{ss} \,, \tag{A.2}$$

see e.g. Deckelnick *et al.* (2005). On noting that

$$\vec{\nabla}_s^2 \left(G'(|\vec{\varkappa}|) \, |\vec{\varkappa}|^{-1} \, \vec{\varkappa} \right) = \vec{\nabla}_s^2 \left(G'(|\varkappa|) \, |\varkappa|^{-1} \, \varkappa \, \vec{\nu} \right) = \left[\left(G'(|\varkappa|) \, |\varkappa|^{-1} \, \varkappa \, \vec{\nu} \right)_s \cdot \vec{\nu} \, \vec{\nu} \right]_s \cdot \vec{\nu} \, \vec{\nu}$$

$$= \left[\left(G'(|\varkappa|) \, |\varkappa|^{-1} \, \varkappa \right)_s \vec{\nu} \right]_s \cdot \vec{\nu} \, \vec{\nu} = \left(G'(|\varkappa|) \, |\varkappa|^{-1} \, \varkappa \right)_{ss} \vec{\nu} \,, \tag{A.3}$$

it is straightforward to establish that (2.14), for $d = 2$, can be formulated as

$$\vec{x}_t \cdot \vec{\nu} = -\left(G'(|\varkappa|) \, |\varkappa|^{-1} \, \varkappa \right)_{ss} + \left[G(|\vec{\varkappa}|) - G'(|\varkappa|) \, |\varkappa| \right] \varkappa + \lambda \, \varkappa \,. \tag{A.4}$$

For the special case (1.3a) with $p = 2$, (A.4) reduces to

$$\vec{x}_t \cdot \vec{\nu} = -\varkappa_{ss} - \tfrac{1}{2} \, \varkappa^3 + \lambda \, \varkappa \,, \tag{A.5}$$

the standard elastic flow in the plane.

We now make the ansatz

$$\vec{x}(\rho, t) = r(t) \left[\cos(2\pi\rho) \, \vec{e}_1 + \sin(2\pi\rho) \, \vec{e}_2 \right] \qquad \forall \, \rho \in I \,, \tag{A.6}$$

with $r(t) > 0$ for all $t \in [0, T]$. It follows from (A.2) that

$$\varkappa(\rho, t) = [r(t)]^{-1} \qquad \forall \, \rho \in I \,\, \forall \, t \in [0, T] \,. \tag{A.7}$$

Moreover, it holds that

$$\vec{x}_t(\rho, t) \cdot \vec{\nu}(\rho, t) = -r'(t) \,. \tag{A.8}$$

Hence a solution of the form (A.6) for the flow (A.4) needs to satisfy

$$\tfrac{1}{2} \frac{\mathrm{d}}{\mathrm{d}t} r^2(t) = G'\!\left(\tfrac{1}{r(t)} \right) \tfrac{1}{r(t)} - G\!\left(\tfrac{1}{r(t)} \right) - \lambda \,. \tag{A.9}$$

The case (1.3a).   Here we obtain the ordinary differential equation

$$\tfrac{1}{2} \frac{\mathrm{d}}{\mathrm{d}t} r^2(t) = \left[\tfrac{1}{r(t)} \right]^{p-1} \tfrac{1}{r(t)} - \tfrac{1}{p} \left[\tfrac{1}{r(t)} \right]^p - \lambda = \left(1 - \tfrac{1}{p} \right) \left[\tfrac{1}{r(t)} \right]^p - \lambda \,. \tag{A.10}$$

It is easy to verify that the solution in the case of $\lambda = 0$ is

$$r(t) = \left[\tfrac{(p-1)\,(p+2)}{p} \, t + r(0)^{p+2} \right]^{\frac{1}{p+2}} \,. \tag{A.11}$$

In particular, for $p \in (1, \infty)$, the solution (A.11) represents expanding circles. For $p = 2$, we obtain the well-known expanding circle solution with radius $r(t) = (2\,t + r(0)^4)^{\frac{1}{4}}$ for elastic flow in the plane.

The case (1.3b). The differential equation (A.9) implies

$$\tfrac{1}{2}\,\frac{\mathrm{d}}{\mathrm{d}t}\,r^2(t) = (\alpha\,r(t) - 1)\,e^{-\alpha\,r(t)} - \lambda\,, \tag{A.12}$$

which for $\lambda = 0$ yields

$$r'(t) = \left(\alpha - \tfrac{1}{r(t)}\right) e^{-\alpha\,r(t)}\,. \tag{A.13}$$

We note that a circle with radius $r = \frac{1}{\alpha}$ is an unstable steady state solution to (A.13), see also the final paragraph below. Circles with a larger radius will (unboundedly) expand, while circles with a smaller radius will shrink (to 0).

If we let $A'(y) = y\,[\alpha\,y - 1]^{-1}\,e^{\alpha\,y}$, we find its antiderivative to be $A(y) = \alpha^{-2}\,(e\,\mathrm{Ei}(\alpha\,y - 1) + e^{\alpha\,y})$, where $\mathrm{Ei}(z) = -\int_{-z}^{\infty} u^{-1}\,e^{-u}\,\mathrm{d}u$ denotes the well-known exponential integral. Then a solution to (A.13), with $r(t) > \frac{1}{\alpha}$, satisfies

$$\frac{\mathrm{d}}{\mathrm{d}t}\,A(r(t)) = r'(t)\,A'(r(t)) = 1\,, \tag{A.14}$$

which means that a solution to (A.13) satisfies the nonlinear equation

$$A(r(t)) = t + A(r(0))\,, \tag{A.15}$$

which can be solved numerically to find $r(t)$.

The case (1.3c). The differential equation (A.9) implies

$$\tfrac{1}{2}\,\frac{\mathrm{d}}{\mathrm{d}t}\,r^2(t) = \left(\alpha\,r(t) - \tfrac{1}{2}\right)\left[\tfrac{1}{r(t)}\right]^{\frac{1}{2}} e^{-\alpha\,r(t)} - \lambda\,, \tag{A.16}$$

which for $\lambda = 0$ yields

$$r'(t) = \left(\alpha - \tfrac{1}{2}\tfrac{1}{r(t)}\right)\left[\tfrac{1}{r(t)}\right]^{\frac{1}{2}} e^{-\alpha\,r(t)}\,. \tag{A.17}$$

We note that a circle with radius $r = \frac{1}{2\,\alpha}$ is an unstable steady state solution to (A.17), see also the final paragraph below. Circles with a larger radius will expand, while circles with a smaller radius will shrink.

Stability of stationary solutions. We observe that for our examples in (1.3) circles of radius $r = |\vec{x}|$ have energy

$$E_\lambda(\vec{x}) = 2\,\pi\left(G\!\left(\tfrac{1}{r}\right) + \lambda\right) r = 2\,\pi\,g_\lambda(r)\,, \quad g_\lambda(r) = \begin{cases} \tfrac{1}{p}\,r^{1-p} + \lambda\,r & \text{(1.3a)} \\ r\,e^{-\alpha\,r} + \lambda\,r & \text{(1.3b)} \\ \sqrt{r}\,e^{-\alpha\,r} + \lambda\,r & \text{(1.3c)} \end{cases}. \tag{A.18}$$

In particular, if $r \to 0$, then only in the case (1.3a) the energy grows unbounded. For the other two cases, circles with radius $r \to 0$ are a minimising sequence for (2.5) if $\lambda \geq 0$.
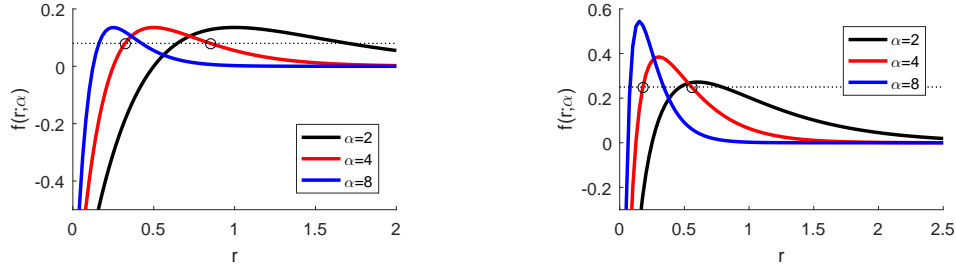
Figure 11: Stationary radial solutions as the intersection of $f(\cdot, \alpha)$, for $\alpha \in \{2, 4, 8\}$, with the line $\lambda =$const (dotted line). The two solutions for $\alpha = 4$ are marked with a circle. The left solution is unstable while the right one is stable. Note that there are no stationary solutions for even moderate $\lambda > 0$. Left: Example (1.3b) with $\lambda = 0.08$. Right: Example (1.3c) with $\lambda = 0.25$.

The radii of stationary radial solutions are now simply the stationary points of g_λ. Their stability can be inferred from the sign change of g_λ', or from the sign of g_λ'', where

$$
g_\lambda'(r) = \begin{cases} \frac{1-p}{p}\, r^{-p} + \lambda \\ e^{-\alpha r}\,(1 - \alpha\, r) + \lambda \\ r^{-\frac{1}{2}}\, e^{-\alpha r}\,(\frac{1}{2} - \alpha\, r) + \lambda \end{cases} \quad \text{and} \quad g_\lambda''(r) = \begin{cases} (p-1)\, r^{-(p+1)} & \text{(1.3a)} \\ \alpha\, e^{-\alpha r}\,(\alpha\, r - 2) & \text{(1.3b)} \\ r^{-\frac{3}{2}}\, e^{-\alpha r}\,(\alpha\, r^2 - \alpha\, r - \frac{1}{4}) & \text{(1.3c)} \end{cases} .
$$
(A.19)

In particular, if r is the radius of a stationary radial solution, i.e. $g_\lambda'(r) = 0$, then for (1.3a) this stationary solution is always stable. For the choice (1.3b) it is stable if $r > \frac{2}{\alpha}$, while for (1.3c) it is stable if $r > \frac{1}{2}\,([1 + \frac{1}{\alpha}]^{\frac{1}{2}} - 1)$. We reformulate the equation $g_\lambda'(r) = 0$ for the stationary radii in the form $f(r, \alpha) = \lambda$ (for examples (1.3b) and (1.3c)) and provide the graph of $f(\cdot, \alpha)$ in Figure 11 for some values of α. It can be seen that there exist no stationary solutions for the cases (1.3b) and (1.3c), and the chosen values of α, if $\lambda > 0$ is too large.

References

Baets, R. and Lagasse, P. E. (1983). Loss calculation and design of arbitrarily curved integrated-optic waveguides. *J. Opt. Soc. Amer.*, **73**(2), 177–182.

Barrett, J. W., Garcke, H., and Nürnberg, R. (2010). Numerical approximation of gradient flows for closed curves in $\mathbb{R}^d$. *IMA J. Numer. Anal.*, **30**(1), 4–60.

Barrett, J. W., Garcke, H., and Nürnberg, R. (2011). The approximation of planar curve evolutions by stable fully implicit finite element schemes that equidistribute. *Numer. Methods Partial Differential Equations*, **27**(1), 1–30.

Barrett, J. W., Garcke, H., and Nürnberg, R. (2012). Parametric approximation of isotropic and anisotropic elastic flow for closed and open curves. *Numer. Math.*, **120**(3), 489–542.

Bartels, S. (2013). A simple scheme for the approximation of the elastic flow of inextensible curves. *IMA J. Numer. Anal.*, **33**(4), 1115–1125.

Bartels, S., Reiter, P., and Riege, J. (2018). A simple scheme for the approximation of self-avoiding inextensible curves. *IMA J. Numer. Anal.*, **38**(2), 543–565.

Dall'Acqua, A., Lin, C.-C., and Pozzi, P. (2017). A gradient flow for open elastic curves with fixed length and clamped ends. *Ann. Sc. Norm. Super. Pisa Cl. Sci. (5)*, **17**(3), 1031–1066.

Davis, T. A. (2004). Algorithm 832: UMFPACK V4.3—an unsymmetric-pattern multifrontal method. *ACM Trans. Math. Software*, **30**(2), 196–199.

Deckelnick, K. and Dziuk, G. (2009). Error analysis for the elastic flow of parametrized curves. *Math. Comp.*, **78**(266), 645–671.

Deckelnick, K. and Grunau, H.-C. (2007). Boundary value problems for the one-dimensional Willmore equation. *Calc. Var. Partial Differential Equations*, **30**(3), 293–314.

Deckelnick, K. and Grunau, H.-C. (2009). Stability and symmetry in the Navier problem for the one-dimensional Willmore equation. *SIAM J. Math. Anal.*, **40**(5), 2055–2076.

Deckelnick, K., Dziuk, G., and Elliott, C. M. (2005). Computation of geometric partial differential equations and mean curvature flow. *Acta Numer.*, **14**, 139–232.

Dziuk, G. (1991). An algorithm for evolutionary surfaces. *Numer. Math.*, **58**(6), 603–611.

Dziuk, G. (1994). Convergence of a semi-discrete scheme for the curve shortening flow. *Math. Models Methods Appl. Sci.*, **4**, 589–606.

Dziuk, G. (2008). Computational parametric Willmore flow. *Numer. Math.*, **111**(1), 55–80.

Dziuk, G., Kuwert, E., and Schätzle, R. (2002). Evolution of elastic curves in $\mathbb{R}^n$: existence and computation. *SIAM J. Math. Anal.*, **33**(5), 1228–1245.

Euler, L. (1952). *Opera Omnia, Ser. 1, 24*. Orell Füssli, Zurich.

Goyal, S., Perkins, N. C., and Lee, C. L. (2005). Nonlinear dynamics and loop formation in Kirchhoff rods with implications to the mechanics of DNA and cables. *J. Comput. Phys.*, **209**(1), 371–389.

Koos, C., Poulton, C. G., Zimmermann, L., Jacome, L., Leuthold, J., and Freude, W. (2007). Ideal bend contour trajectories for single-mode operation of low-loss overmoded waveguides. *IEEE Photon. Technol. Lett.*, **19**(11), 819–821.

Lindenmann, N., Balthasar, G., Hillerkuss, D., Schmogrow, R., Jordan, M., Leuthold, J., Freude, W., and Koos, C. (2012). Photonic wire bonding: a novel concept for chip-scale interconnects. *Opt. Express*, **20**(16), 17667–17677.

Marcuse, D. (1993). Bend loss of slab and fiber modes computed with diffraction theory. *IEEE J. Quantum Electron.*, **29**(12), 2957–2961.

Mio, W., Srivastava, A., and Klassen, E. (2004). Interpolations with elasticae in Euclidean spaces. *Quart. Appl. Math.*, **62**(2), 359–378.

Negredo, F., Blaicher, M., Nesic, A., Kraft, P., Ott, J., Dörfler, W., Koos, C., and Rockstuhl, C. (2018). Fast and reliable method to estimate losses of single-mode waveguides with an arbitrary 2D trajectory. *J. Opt. Soc. Am. A*, **35**(6), 1063–1073.

Polden, A. (1996). *Curves and surfaces of least total curvature and fourth-order flows*. Ph.D. thesis, University Tübingen, Tübingen.

Schätzle, R. (2010). The Willmore boundary problem. *Calc. Var. Partial Differential Equations*, **37**(3-4), 275–302.

Schmidt, A. and Siebert, K. G. (2005). *Design of Adaptive Finite Element Software: The Finite Element Toolbox ALBERTA*, volume 42 of *Lecture Notes in Computational Science and Engineering*. Springer-Verlag, Berlin.

Tröltzsch, F. (2010). *Optimal Control of Partial Differential Equations: Theory, Methods and Applications*, volume 112 of *Graduate Studies in Mathematics*. American Mathematical Society, Providence, RI.

Tu, Z. C. and Ou-Yang, Z. C. (2008). Elastic theory of low-dimensional continua and its applications in bio- and nano-structures. *J. Comput. Theor. Nanosci.*, **5**(4), 422–448.